Hindawi
Shock and Vibration
Volume 2018, Article ID 5731347, 22 pages
https://doi.org/10.1155/2018/5731347

Research Article

A Reduced-Order Model for Active Suppression Control of Vehicle Longitudinal Low-Frequency Vibration

Donghao Hao,[1] **Changlu Zhao**,[1] **and Ying Huang**[1,2]

[1]*Research Center of Power Machinery, Beijing Institute of Technology, Beijing 100081, China*
[2]*Beijing Collaborative Innovation Center for Electric Vehicles, Beijing 100081, China*

Correspondence should be addressed to Ying Huang; hy111@bit.edu.cn

Received 26 June 2017; Accepted 12 December 2017; Published 8 January 2018

Academic Editor: Sergio De Rosa

Establishing a prediction model, with linearity and few dof (degree of freedom), is a key step for the design of a control algorithm based on the modern control theory. In this paper, such a model is needed for active suppression of vehicle longitudinal low-frequency vibration. However, many dynamic processes in the vehicle have different effects on the vibration. Therefore, a detailed coupling model is firstly established, considering the dynamics of the torsional vibrations of the driveline and the tire, the tire force nonlinearity, and the vehicle vertical and pitch vibrations. Based on this model, sensitivity analysis is conducted and the results show that the tire slip, the torsional stiffness of the half-shaft, and the tire have great influences on the longitudinal vibration. Then a three-dof model is obtained by linearizing the tire slip into damping. A parameter estimation method is designed to obtain the model parameters. Finally, the model is validated. The time domain response, error analysis, and frequency response results demonstrate that the 3-dof model has a good consistency with the detailed coupling model. It is suitable as a control-oriented model.

1. Introduction

With the development of the automotive industry, there is a growing emphasis on the quality of automobile, of which drivability is the key factor. The longitudinal low-frequency (0–10 Hz) vibration of the vehicle is an important part in drivability evaluation [1] as shown in Figure 1. Therefore, it is an automotive NVH research focus. Usually, longitudinal low-frequency vibration is characterized by frequency and attitude or power spectrum of vehicle longitudinal acceleration or jerk (the derivative of acceleration), which happens with greater amplitude in some transient operating conditions, such as rapid acceleration and emergency deceleration [2]. Due to the resonant frequency of the human organs in this range, passengers are more sensitive to vehicle low-frequency vibration, resulting in a serious dissatisfaction with the comfort [3]. Therefore, in order to improve drivability and comfort, it is necessary to solve the problem of vehicle longitudinal low-frequency vibration.

In recent years, a large number of studies on this issue have been carried out at home and abroad, which focus on the mechanisms and vibration control methods of this phenomenon. In respect of mechanism, Rabeih and Crolla [4] have studied on the mechanism and influence factors. He pointed out that longitudinal low-frequency vibration is mainly excited by the first-order torsional vibration of driveline and could be disturbed by the vertical vibration of suspensions. A sudden change in the engine torque causes the torsional vibration of the transmission system, resulting in fluctuation in the drive torque of the wheel, which in turn affects the vehicle longitudinal acceleration. Transmission ratio, flywheel quality, vehicle quality, transmission stiffness, and damping have different impacts on the frequency and amplitude of vehicle longitudinal vibration. However, this article does not reveal the interaction between the tire longitudinal force and the suspension vertical force during tip-in process. In addition, a quarter car model used in this article does not consider the effect of the pitch vibration on the tire longitudinal force during acceleration. Sorniotti of the University of Surrey in the UK [5] pointed out that the main factors affecting the vehicle longitudinal low-frequency vibration were the stiffness of the driveshaft and half-shaft. The vibration frequency differs under different gears, such as high-frequency vibration under high gear. Crowther and

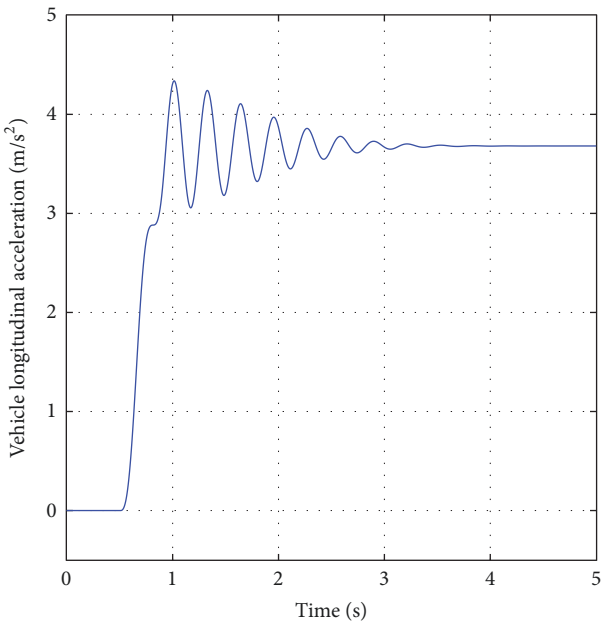

Figure 1: Vehicle response in a tip-in condition: vehicle longitudinal acceleration.

Zhang in Sydney University of Science and Technology [6] pointed out that many nonlinear factors, such as clutch friction characteristics, transmission shaft clearance, and tire stiffness, had greater impacts on longitudinal low-frequency vibration. It is found that the frequency of longitudinal vibration mainly depends on the engine output torque increase rate, gear position, and engine flywheel mass moment of inertia through experiments [7]. In addition, the literature [8] has studied the effect of road surface on the half-shaft torque fluctuation, indicating that the vibration frequency and amplitude of the half-shaft torque are closely related to the conditions of the road surface. From this point of view, road conditions may influence the vehicle longitudinal vibration.

In the aspect of the longitudinal low-frequency vibration suppression, active compensation of engine (internal combustion engine vehicle) or motor (electric or hybrid vehicle) torque has been developed and adopted by many scholars and automotive companies. There are two main methods including open-loop and closed-loop control. The concept of open-loop control is the limit of the engine torque increase rate. That is, a torque increase rate limitation is obtained by querying the MAP under a certain operating condition and is applied in engine torque control. This method is generally used by automotive companies, especially in avoiding the impact of the transmission system through the backlash, which could increase the amplitude of longitudinal vibration. Nevertheless, the effectiveness of this control method depends entirely on the subjective idea of the calibration engineers. At the same time, a large number of MAPs need to be calibrated to cover torque rate limitation at different gear, different engine speed, and different accelerator pedal position, which consumes a lot of development time. Taking into account the above deficiencies, there are more automotive companies tending to develop automatic closed-loop control method to suppress the longitudinal low-frequency vibration gradually. Closed-loop control is divided into non-model-based and model-based control methods. The former does not require accurate power transmission system and vehicle models. With the calibration of the PID three parameters, a certain indicator is tracked to reduce the vibration amplitude of longitudinal acceleration. The indicators mainly include the speed difference (the engine flywheel speed divided by whole transmission ratio, then subtracting wheel speed, and it is abbreviated as "speed difference" in this paper) [9] and the fluctuation components of engine speed [10, 11]. These control methods execute and take effect only when the vibration is detected. In other words, the longitudinal vibration has happened already. Therefore, there is a certain control delay and the vibration suppression effectiveness is limited. The model-based closed-loop control method, which is applied to the vehicle longitudinal low-frequency vibration control, mainly includes the pole placement method based on modern control theory [12, 13], the root locus method based on classical control theory [14], and the method based on optimal control theory [15, 16]. This kind of control algorithm has the advantages of high portability, less reliance on experimental calibration, and high control precision. However, since the control output depends on the optimization of the state or output variables, which are calculated from the established system model in real time, the accuracy of the model has considerable impact on the control effectiveness. In addition, in order to reduce the hardware overhead of the control system and simplify the structures of the control algorithm, the dynamic model should have fewer orders. Nevertheless, this demand contradicts the model accuracy. Therefore, the establishment of a linear model, having few degrees of freedom and high consistency with real longitudinal vibration process, will be the prerequisite for the successful design of the longitudinal vibration suppression algorithm based on modern control theory.

In order to design a controller to suppress the longitudinal low-frequency vibration, a two-degree-of-freedom vehicle longitudinal vibration model was established, in which engine flywheel, clutch, gearbox, and drive shaft are equivalent to one inertia and the wheel is equivalent to the second inertia. The wheel inertia is affected by the load, which consists of the rolling resistance, air drag, and vehicle mass. The two equivalent inertias are connected by the half-shaft with stiffness and damping. Based on this model, a third-order state space equation was designed [16]. Literatures [14, 17] also used the double-inertia model for longitudinal vibration control. Although the amplitude of acceleration fluctuation decreases, obvious fluctuation still can be seen from the results. A different type of dual-inertia model was designed. The differences are that the second inertia was equivalent to the inertia of vehicle mass and an equivalent damping, representing the tire dynamics, was connected in series to half-shaft [18]. Also, a dual-inertia model was expressed in the form of a transfer function to design controller in literature [19]. In literature [20], a three-inertia model was established and the three inertias were connected

by two shafts with torsional stiffness and damping. The model parameters were obtained by an identification method and the accuracy is compared with a dual-inertia model. However, the model does not take into account the tire torsional stiffness and slip, which indeed have obvious impacts on longitudinal vibration. Therefore, the control results based on this model showed a certain acceleration vibration. In the literature [8], a number of longitudinal vibration models with different degrees of freedom were established. The simulation results showed that the model, considering tire torsional dynamic, could reflect the real longitudinal acceleration fluctuation, whereas obtaining method of model parameters and design of reduced-order model were not involved.

In summary, it is very important to establish a few degree-of-freedom linear dynamic model which can reflect the dynamic process of vehicles longitudinal vibration, which has considerable influence on the control effectiveness of the vibration suppression controller based on the modern control theory. Therefore, the modeling of a control-oriented vehicle longitudinal low-frequency vibration model will be the focus of this paper. Firstly, a detailed multi-degree-of-freedom vehicle longitudinal vibration dynamic model is established, considering the torsional vibration of the transmission system and tire, the nonlinear longitudinal force of the tire, and the pitch and vertical vibration of the suspension. Based on this model, the sensitivity of different influence factors on the longitudinal vibration, consisting of the internal stiffness of the clutch, stiffness of the half-shaft, torsional dynamic of tire, nonlinear force of tire, and pitch vibration caused by the stiffness of the suspension, is analyzed. Then the main factors affecting the longitudinal vibration are obtained. Afterwards two reduced-order models, simplified from the detailed multi-degree-of-freedom vehicle model, are established and satisfy the modeling requirements of modern control theory. One part of the model parameters is derived from the vehicle parameters based on the lumped-mass method and law of the conservation of energy and other parts of those parameters are obtained by means of parameter estimation method. Finally, the consistency of the simplified model with detailed model is verified. As a result, the three-degree-of-freedom model can reflect the vehicles longitudinal low-frequency vibration accurately.

This paper is mainly composed of the following five sections. In Section 2, a detailed multi-degree-of-freedom vehicle longitudinal vibration model is established, considering the dynamics of transmission system, tire, suspension, and vehicle body, which can reflect the characteristics of vehicle longitudinal low-frequency vibration. In Section 3, the sensitivity of the influences of different components and parameters on longitudinal vibration are analyzed and the main influence factors are analyzed. Section 4 shows the reduced-order model, model reduction method, and model parameters obtained method. Section 5 verifies the consistency of the simplified model. Section 6 summarizes the full text.

2. Coupling Model of Vehicle Longitudinal Vibration

The research object is a front-engine-front-wheel-drive vehicle, in which the engine output torque is transmitted to driving wheels through the clutch, gearbox, differential and half-shaft. Longitudinal force from the ground is applied on the driving wheels and is transmitted through the swing arm, bushing, and vehicle frame to drive the vehicle. The longitudinal acceleration depends largely on the rotational acceleration of the driving wheels, determined by the combined action of the half-shaft torque and the ground longitudinal force. Torque fluctuation of the half-shaft is mainly influenced by the elastic characteristics of the driveline and excitation torque of the engine while the longitudinal force applied on the driving wheels is effected by the tire slip and tire vertical force. In tip-in condition, the engine torque with rapid increase rate causes torque fluctuation of the half-shaft, which makes the torsional acceleration of driving wheels fluctuate. This will cause slip ratio and longitudinal force to fluctuate. This fluctuation in turn exacerbates torsional vibration of driving wheels and longitudinal vibration of wheel center, affecting vehicle longitudinal vibration. In addition, in tip-in condition, the load transfer between the front and rear wheels as well as the vertical stiffness of the suspensions and tires will cause tire vertical force to fluctuate, which alters road adhesion condition and longitudinal force. This can aggravate wheel torsional vibration and vehicle longitudinal vibration.

It can be seen that the longitudinal low-frequency vibration transfer path is the engine-transmission system-tire-ground-bushing-body, in which the longitudinal force between the tire and ground is affected by suspension vibration, as shown in Figure 2.

Figure 2 shows that vehicle longitudinal vibration is a coupling vibration of the transmission system torsional vibration, tire nonlinear vibration, and suspension vertical and body pitch vibration. Therefore, vibrations of the three parts should be taken into account to build the longitudinal vibration dynamic model.

2.1. Powertrain Torsional Vibration Submodel. The structure of the power transmission system is shown in Figure 3, consisting of the engine (denoted by subscript e), the clutch (denoted by subscript c), the gearbox (denoted by subscripts $g1$, $g2$, representing a pair of meshing gears), the differential (denoted by subscript df), the half-shaft (denoted by subscript hs), the hub (including rim and brake disc denoted by subscript rim), and the tire (denoted by subscript t). The sign θ represents the angular displacement. J is the mass moment of inertia and T is the torque. Subscripts r and l represent right and left. f and r represent front and rear. Detailed definition of all the symbols are given in Table 5.

T_e is the engine output torque. T_c is the clutch torque (induced by torsional shock absorber). J_e is the engine flywheel inertia. The engine flywheel satisfies the following kinetic equation:

$$T_e - T_c = J_e \ddot{\theta}_e. \tag{1}$$

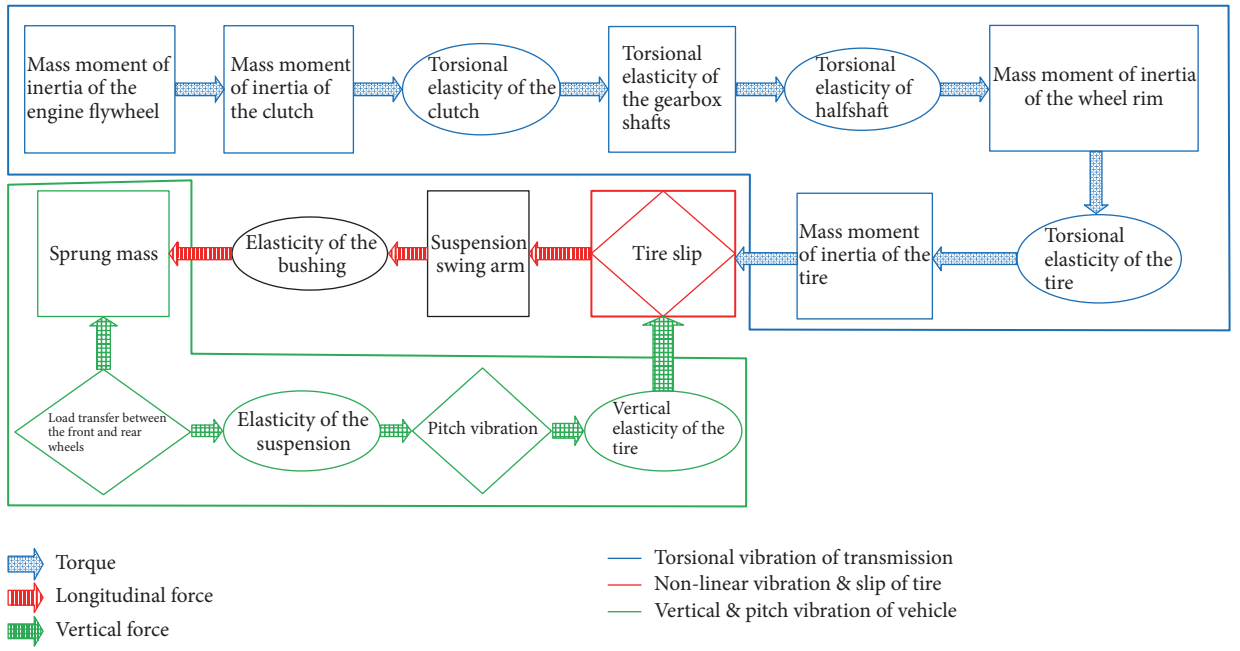

Figure 2: Vehicle longitudinal low-frequency vibration transfer path.

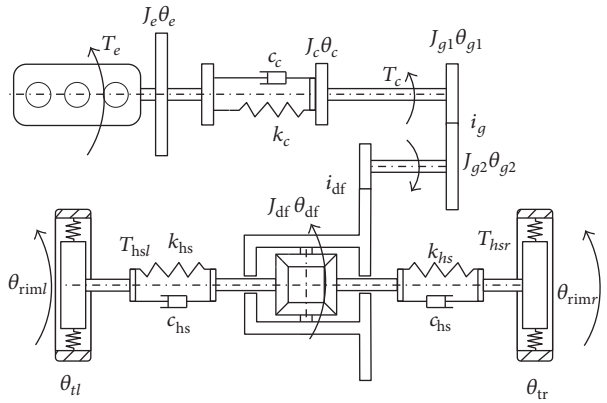

Figure 3: Structure of driveline.

In a fixed gear position, where the clutch is always in the engaged state, ignoring the clutch slip phenomenon, the clutch torque meets

$$T_c = k_c\left(\theta_e - \theta_{g1}\right) + c_c\left(\dot{\theta}_e - \dot{\theta}_{g1}\right). \tag{2}$$

Gearbox input and output shaft are short and the stiffness of the shaft and gear are relatively large. Therefore, the elasticity of gearbox shafts is ignored and considered as rigid connection. The clutch, gearbox input shaft, gears, output shaft, and differential output shaft are lumped together as one moment of inertia, J_{d}. It satisfies

$$J_{\mathrm{d}}\ddot{\theta}_{\mathrm{df}} = T_c i_g i_{\mathrm{df}} - T_{\mathrm{hs}} \tag{3}$$

with J_{d} given by

$$J_{\mathrm{d}} = {i_g}^2{i_{\mathrm{df}}}^2\left(J_{g1} + J_c\right) + {i_{\mathrm{df}}}^2 J_{g2} + J_{\mathrm{df}}. \tag{4}$$

T_{hs} is the torque of the half-shaft calculated by

$$\begin{aligned} T_{\mathrm{hs}} &= T_{\mathrm{hs}r} + T_{\mathrm{hs}l}, \\ T_{\mathrm{hs}r} &= k_{\mathrm{hs}}\left(\theta_{\mathrm{df}} - \theta_{\mathrm{rim}r}\right) + c_{\mathrm{hs}}\left(\dot{\theta}_{\mathrm{df}} - \dot{\theta}_{\mathrm{rim}r}\right), \\ T_{\mathrm{hs}l} &= k_{\mathrm{hs}}\left(\theta_{\mathrm{df}} - \theta_{\mathrm{rim}l}\right) + c_{\mathrm{hs}}\left(\dot{\theta}_{\mathrm{df}} - \dot{\theta}_{\mathrm{rim}l}\right). \end{aligned} \tag{5}$$

Assuming the differential is locked and wheels in both sides have the same condition, the wheel rotation speed and torque can be expressed as

$$\begin{aligned} \dot{\theta}_{\mathrm{rim}r} &= \dot{\theta}_{\mathrm{rim}l}, \\ T_{\mathrm{hs}l} &= T_{\mathrm{hs}r}. \end{aligned} \tag{6}$$

2.2. Tire Submodel. The tire is modeled in this study based on the same principle of a published work in this area by Sharp and Jones [21], Pacejka [22], and Bartram et al. [8], which includes the tire torsional stiffness and the vertical stiffness, expressed as k_t and k_{tf}, respectively, as shown in Figure 4. The hub, the rim, and the brake disc are lumped together as one rotating inertia due to the rigid connection. J_{tire} is the tire inertia. M_b is the sprung mass. The wheel rim is connected to the vehicle body through the vertical and longitudinal springs and dampers.

This paper mainly studies the vehicle longitudinal low-frequency vibration under start-up tip-in condition, in which the rolling resistance can be neglected due to low wheel speed. The rear wheels are passive driven, considered as a part of the body quality. The equation for the driving wheel hub is

$$J_{\mathrm{rim}}\ddot{\theta}_{\mathrm{rim}} = T_{\mathrm{hs}} - T_{\mathrm{tire}}. \tag{7}$$

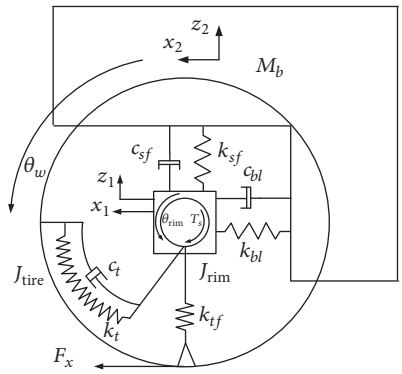

Figure 4: Model of tire and its connection with vehicle body.

The equation for the tire is

$$J_{\text{tire}}\ddot{\theta}_w = T_{\text{tire}} - T_{tf} - T_r, \tag{8}$$

where T_{tf} is the driving torque generated from the ground and defined as

$$T_{tf} = F_x \cdot r. \tag{9}$$

r is the effective wheel rolling radius.

T_{tire} is the torque transferred from the rim to the tire, caused by the angular displacement deviation of the elastic tire, calculated by

$$T_{\text{tire}} = k_t\left(\theta_{\text{rim}} - \theta_w\right) + c_t\left(\dot{\theta}_{\text{rim}} - \dot{\theta}_w\right). \tag{10}$$

The longitudinal force applied on the tire from the ground is nonlinear, which can be calculated by the Magic Tire Formula. The Magic Tire Formula has high consistency with the experimental data. The longitudinal force F_x is calculated as follows:

$$\begin{aligned} F_x = f\left(s_t, F_z\right) = F_z \cdot D \cdot \sin\big(C \\ \cdot \arctan\left(B \cdot s_t - E\left(B \cdot s_t - \arctan\left(B \cdot s_t\right)\right)\right)\big). \end{aligned} \tag{11}$$

The four parameters (B, C, D, E) represent the nonlinearity characteristics of the tire longitudinal force, which together determine the stiffness, the shape, the peak, and the curvature of the friction coefficient-slip curve. F_z is the vertical force, of which value varies with the vertical vibration of the tire and the suspension. It is derived in the next chapter. s_t is the tire slip ratio, defined as follows:

$$s_t = \frac{\dot{\theta}_w r - \dot{x}_1}{\dot{\theta}_w r}, \tag{12}$$

where $\dot{x}_1$ is the longitudinal speed of the rim center and $\dot{\theta}_w$ is the rotating speed of the tire.

Since the longitudinal force between the tire and the vehicle body is mainly transmitted through the bushing, vehicle longitudinal vibration is closely related to the elastic characteristics of the bushing. The longitudinal dynamics relationship between the wheel and the vehicle body is shown as

$$\begin{aligned} M_w\ddot{x}_1 &= F_x - F_b, \\ \frac{M_b}{2}\ddot{x}_2 &= F_b, \end{aligned} \tag{13}$$

$$F_b = k_{bl}\left(x_2 - x_1\right) + c_{bl}\left(\dot{x}_2 - \dot{x}_1\right), \tag{14}$$

where x_1 is the longitudinal displacement of the rim mass center and x_2 is the longitudinal displacement of the vehicle mass center. F_b is the longitudinal force applied between the body and the wheel. k_{bl} and c_{bl} are the stiffness and damping coefficients of the bushing, respectively.

2.3. Vehicle Body Vertical and Pitch Motion Submodel. In tip-in condition, the driving wheel is subjected to a large longitudinal force from the ground. Due to the moment balance relationship, the front part of the vehicle has a tendency to rotate clockwise around the vehicle mass center while the rear part of the vehicle has a tendency to rotate counterclockwise, which induces load transfer between the front half-shaft and the rear half-shaft. Vehicle body pitch vibration will be generated due to the shaft load transfer as well as the vertical reciprocating movement of the elastic suspension and tire, which induces the vertical force between tire and ground to fluctuate. As the above considerations, a half-car model is established which is symmetrical with the x-axis, as shown in Figure 5.

The stiffness and damping coefficients of the front suspension are k_{sf} and c_{sf} while those of the rear suspension are k_{sr} and c_{sr}. The vertical stiffness coefficients of the front and the rear tire are k_{tf} and k_{tr} while the mass of the front and the rear wheel are M_{wf} and M_{wr}. In all the work conditions, we assume that all wheels keep contact with the ground. J_b is the mass moment of inertia of the sprung mass around the pitch center. The distance between the front shaft and the vehicle mass center is a and that between the rear shaft and the vehicle mass center is b.

The dynamic equations of the sprung mass are

$$\begin{aligned} \frac{M_b}{2}\ddot{z}_b &= F_f + F_r - \frac{M_b}{2}g, \\ J_b\ddot{\theta}_b &= -aF_f + bF_r - F_b\left(h - r\right). \end{aligned} \tag{15}$$

The vertical motion equations of the front and the rear tires are

$$\begin{aligned} M_{wf}\ddot{z}_{tf} &= k_{tf}\left(z_{tf(0)} - z_{tf}\right) - F_f, \\ M_{wr}\ddot{z}_{tr} &= k_{rf}\left(z_{rf(0)} - z_{rf}\right) - F_r. \end{aligned} \tag{16}$$

The vertical force of the front and the rear suspensions are calculated as follows:

$$\begin{aligned} F_f &= k_{sf}\left(z_{sf} - z_{tf} - z_{sf(0)}\right) + c_{sf}\left(\dot{z}_{sf} - \dot{z}_{tf}\right), \\ F_r &= k_{sr}\left(z_{sr} - z_{tr} - z_{sr(0)}\right) + c_{sr}\left(\dot{z}_{sr} - \dot{z}_{tr}\right), \end{aligned} \tag{17}$$

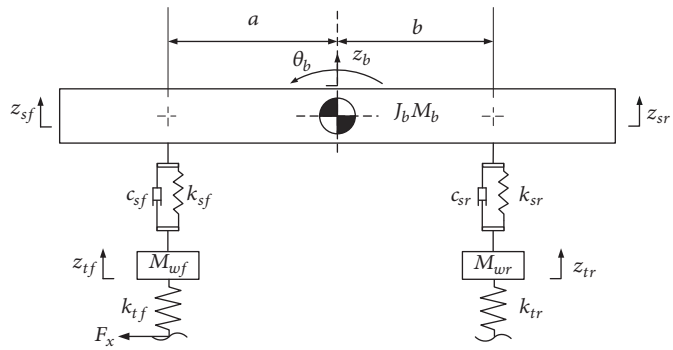

Figure 5: Suspension vertical and vehicle body pitch vibration model.

where the initial values of z_{tf}, z_{sf}, z_{tr}, and z_{sr} are defined as follows:

$$\begin{aligned} z_{tf(0)} &= \frac{M_w g + 0.5 M_b b g / (a+b)}{k_{tf}}, \\ z_{sf(0)} &= \frac{M_b b g}{2(a+b)k_{sf}}, \\ z_{tr(0)} &= \frac{M_w g + 0.5 M_b a g / (a+b)}{k_{tr}}, \\ z_{sr(0)} &= \frac{M_b a g}{2(a+b)k_{sr}}. \end{aligned} \tag{18}$$

Assuming the pitch angle is small, the kinetic equations of the sprung mass are valid as follows:

$$\begin{aligned} \ddot{z}_{sf} &= \ddot{z}_b - a\ddot{\theta}_b, \\ \ddot{z}_{sr} &= \ddot{z}_b + b\ddot{\theta}_b. \end{aligned} \tag{19}$$

3. Sensitivity Analysis of Longitudinal Low-Frequency Vibration

The deviation of parameters value between the control-oriented simplified model and the real system lead to output errors between the model and the real physical system, which will have serious effect on the control effectiveness. This deviation is caused by the parameter measurement error and the neglect of some dynamic process in the reduced-order model. Therefore, sensitivity analysis is conducted in our study. It can obtain the sensitivity of the longitudinal low-frequency vibration responses to the variation of the system parameters, deciding the system parameters which have great influence on the longitudinal vibration. This can provide the theoretical basis for the simplification of the multi-degree-of-freedom nonlinear model and the analysis of the modeling error of the reduced model. As the longitudinal low-frequency vibration occurs mainly in tip-in condition, a ramp torque is considered as excitation in the sensitivity analysis process, as shown in Figure 6. The ramp rate is 400 Nm/s and the final value is 200 Nm.

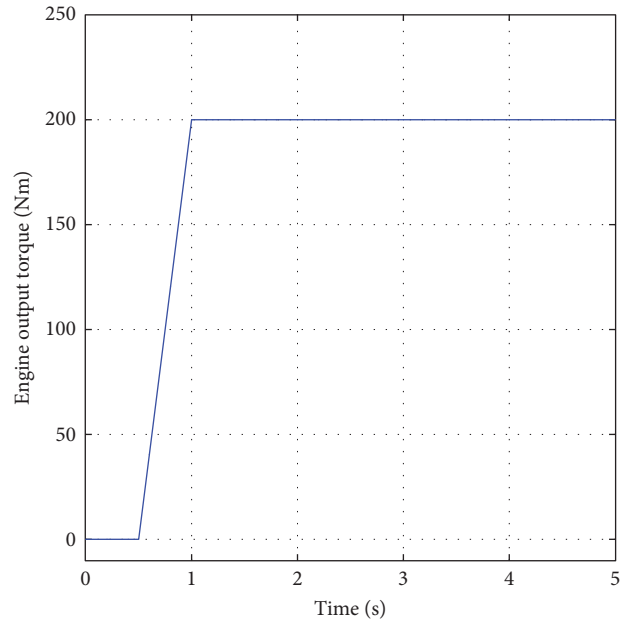

Figure 6: Engine output torque.

3.1. Sensitivity Analysis of the Driveline. Assuming that the backlash of a pair of gears is traversed and the gearbox is in a fixed gear, we analyze the influence of the main elastic parts in the driveline on the longitudinal low-frequency vibration, such as the clutch and the half-shaft.

3.1.1. Clutch. The clutch and the internal torsion spring interrupt the transfer of power and change the natural frequency of the driveline. The internal torsion springs are generally composed of several springs with different torsional stiffness, considered as a nonlinear part. By changing the stiffness and damping of springs, the sensitivity of the vehicle longitudinal acceleration to the clutch parameter is analyzed. The nominal stiffness and damping coefficients of the clutch are 1000 Nm/rad and 20 Nm/(rad/s), respectively. In the range of normal value, 0.5, 1, and 2 times the nominal coefficients are set as system parameters in each simulation. The stiffness coefficient of the clutch is 500 Nm/rad, 1000 Nm/rad, and

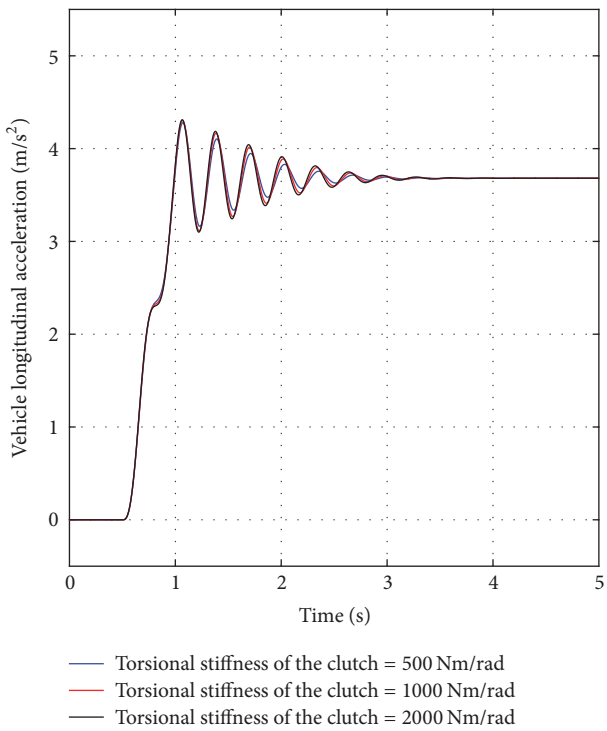

FIGURE 7: Sensitivity analysis: effect of the variation of the torsion stiffness k_c of the clutch.

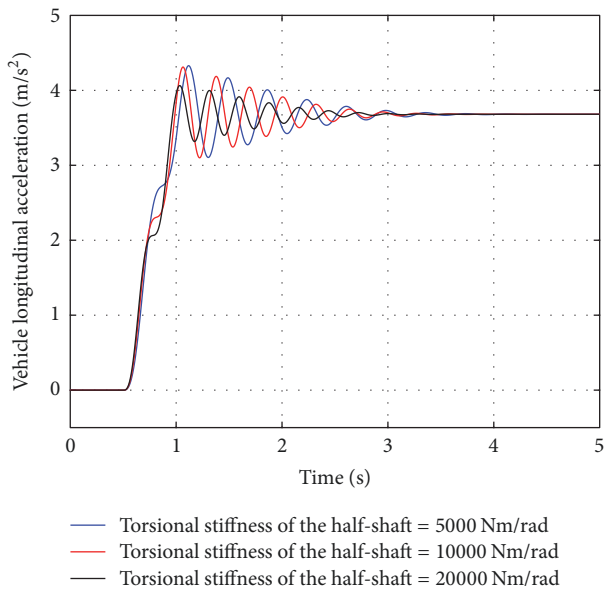

FIGURE 8: Sensitivity analysis: effect of the variation of the torsion stiffness k_{hs} of the half-shaft.

2000 Nm/rad in sequence. The simulation results are shown in Figure 7.

It can be seen from the figure that the amplitude and frequency of the acceleration vibration increase with the increase of the clutch torsional stiffness, although the change is very small. The damping coefficient has a similar conclusion, omitted here. Based on the fact that the variation of the clutch stiffness and damping have little influence on the longitudinal low-frequency vibration, the nonlinear torsional stiffness and damping of the clutch can be replaced with a fixed value in the reduced-order model.

3.1.2. Half-Shaft. Keeping other parameters unchanged, by only changing the stiffness of the half-shaft, the sensitivity of the acceleration vibration to the half-shaft stiffness and damping coefficient is analyzed. The nominal stiffness and damping coefficients of the half-shaft are 10000 Nm/rad and 40 Nm/(rad/s), respectively. In the range of normal value, 0.5, 1, and 2 times the nominal coefficients are set as system parameters in each simulation. The stiffness coefficient of the half-shaft is 5000 Nm/rad, 10000 Nm/rad, and 20000 Nm/rad in sequence. Sensitivity analysis results are shown in Figure 8.

It can be seen that the longitudinal vibration frequency increases as the torsional stiffness increases. Compared with Figure 7, the influence of the stiffness variation of the half-shaft is more obvious than that of the clutch. It is because that the rise rate of the half-shaft torque is more than ten times greater than that of the engine torque which passes through the gearbox and the differential, increasing twice, especially in the first gear. The torque with greater rise rate will cause larger torsional deformation of the half-shaft, which induces obvious torque fluctuation. This makes the acceleration vibration change seriously. On the contrary, the clutch shaft torsional deformation changes insignificantly with the variation of the torsional stiffness, due to the smaller rise rate of the torque on the clutch shaft. This induces smaller torque fluctuation and leads to little change of the acceleration vibration. The same conclusion applies to the damping coefficient, detailed simulation omitted here for simplicity.

To sum up, the stiffness and damping variations of the clutch and the half-shaft must be taken into account in the establishment of a control-oriented vehicle longitudinal vibration model. More importantly, the accuracy of the half-shaft stiffness coefficient has a great influence on the states and outputs accuracy of the reduced-order model to be established.

3.2. Sensitivity Analysis of the Tire. The tire characteristics, including the torsional stiffness, the nonlinear longitudinal force, and the vertical vibration, have a certain effect on the longitudinal vibration. However, in some literatures on the longitudinal vibration, the tire torsional elasticity and the tire slip characteristics are not considered in detail [18]. In this part, the influence of the tire torsional stiffness and slip on longitudinal vibration are studied firstly and then the sensitivity analysis of the two factors is conducted. Since the vertical stiffness of the tire is closely related to the vertical vibration of the suspension, it will be analyzed together with suspension in Section 3.3.

3.2.1. Torsional Stiffness of the Tire. As (10) shows, k_t is the equivalent torsional stiffness of the tire, which connects the hub inertia J_{rim} to the tire inertia J_{tire}. The nominal value of k_t

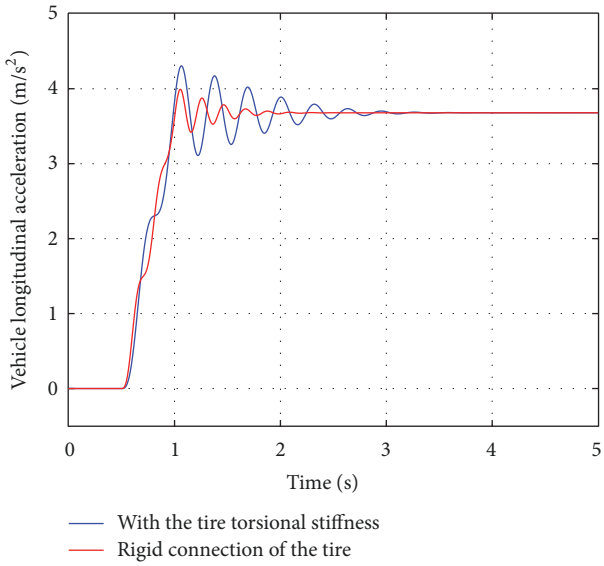

Figure 9: Longitudinal acceleration of the model with/without the tire torsional stiffness.

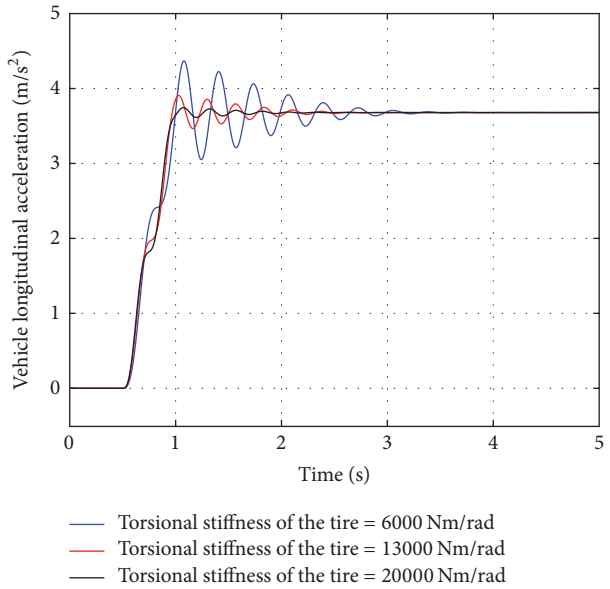

Figure 10: Sensitivity analysis: effect of the variation of the torsion stiffness k_t of the tire.

is 13000 Nm/rad. Here the influence of the torsional stiffness of the tire on the longitudinal vibration is studied as shown in Figure 9. The blue line is the longitudinal acceleration with tire torsional stiffness while the red line is the longitudinal acceleration with the rigid connection between the wheel hub and the tire.

It can be seen that the longitudinal vibration frequency is larger and the overshoot is smaller in the model with the rigid connection between the wheel hub and the tire, compared with the model with tire torsional stiffness.

In the range of normal value, 0.5, 1, and 2 times the nominal coefficients are set as system parameters in each simulation. The torsional stiffness coefficient of the tire is 6000 Nm/rad, 13000 Nm/rad, and 20000 Nm/rad in sequence. Sensitivity analysis results are shown in Figure 10.

It can be seen that the variation of the tire torsional stiffness has a significant effect on the longitudinal acceleration. The fluctuation amplitude of the longitudinal acceleration decreases obviously while the frequency increases slightly with the increase of the tire torsional stiffness. Therefore, the tire torsional stiffness must be taken into account in the establishment of control-oriented driveline and vehicle longitudinal vibration model.

3.2.2. Relationship between the Tire Slip Ratio and the Friction Coefficient. As mentioned before, few studies considered the effects of the tire slip on vehicle longitudinal vibration. However, due to the phase asynchronization between the tire rotation speed and the vehicle longitudinal speed, which is caused by the tire slip, the speed measured from the speed sensor on the wheel hub will not accurately reflect the vehicle longitudinal acceleration fluctuation. The deviation between the tire rotation speed and the body longitudinal speed increases dramatically in tip-in condition due to the large longitudinal deformation of the tire caused by the torque with rapid increase rate. Therefore, the effect of the tire slip

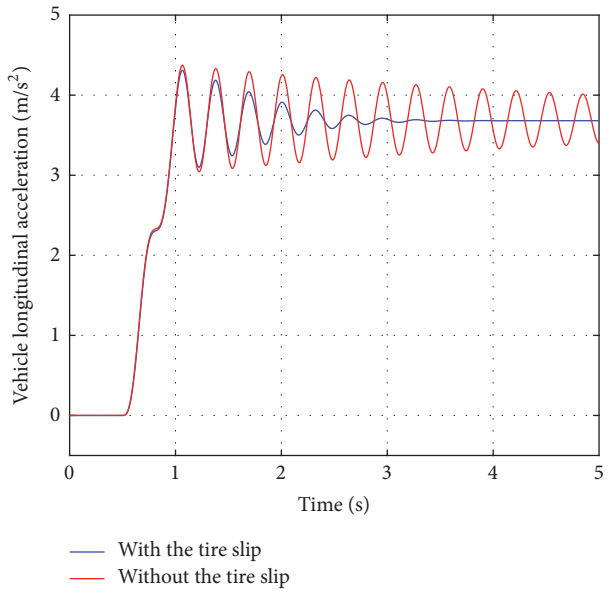

Figure 11: Longitudinal acceleration of the model with/without the tire slip.

must be studied and the results are shown in Figure 11. The blue line is the longitudinal acceleration of the detailed vehicle model with wheel slip ratio variation while the black line is the longitudinal acceleration of the detailed vehicle model ignoring the wheel slip. In other words, the wheel slip ratio keeps zero in the second model, in which the tire rotation speed and the vehicle longitudinal speed keep synchronous.

The blue line in Figure 11 shows that the vehicle longitudinal acceleration gradually stabilizes due to the tire slip. However, the longitudinal acceleration keeps fluctuating in

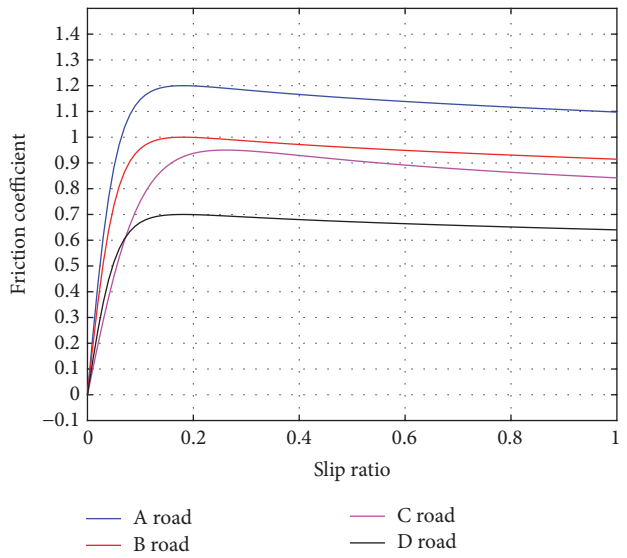

Figure 12: Slip ratio-friction coefficient curve in the four road conditions.

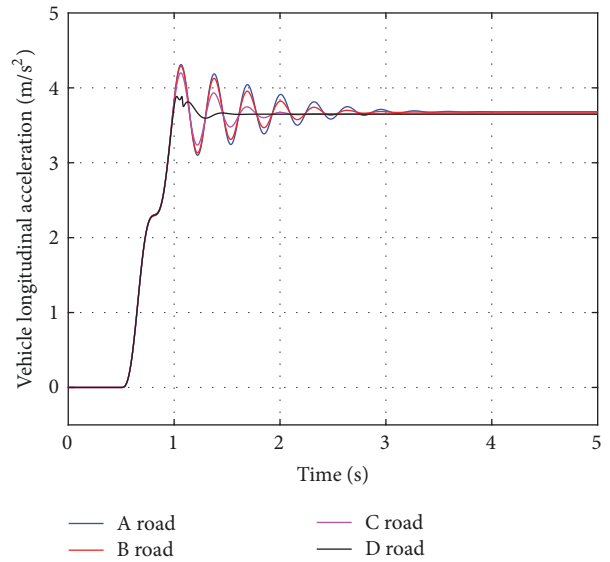

Figure 13: Sensitivity analysis: effect of the variation of slip condition.

Table 1: Magic Tire Formula parameters in the four road conditions.

Road conditions	B	C	D	E
A	10	1.9	1.2	0.97
B	10	1.9	1	0.97
C	5	2.1	0.9	0.97
D	10	1.9	0.8	0.97

the model with zero slip ratio, shown as red line in Figure 11, which is seriously inconsistent with the real physical system. Therefore, the tire slip characteristic must be considered in the establishment of control-oriented vehicle longitudinal vibration model.

Since the slip ratio value is not equal to zero in real driving conditions and varies from the road adhesion conditions and tire materials, four different road adhesion conditions are established. Tip-in condition is conducted on the four roads separately to investigate the sensitivity of the vehicle longitudinal vibration to the relationship variation between the slip ratio and the friction coefficient. The parameters of the Magic Tire Formula for the four road conditions are shown in Table 1 and the corresponding slip ratio-friction coefficient curve is shown in Figure 12. These four different road conditions represent the relationship variation between the slip ratio and the friction coefficient.

Sensitivity analysis results are shown in Figure 13.

Lines A, B, and C in Figure 13 show that the variation of the tire adhesion condition has a significant effect on the longitudinal acceleration vibration, especially on amplitude. The longitudinal deformation of the tire tends to be larger with the increase of adhesion coefficient, which induces larger fluctuation of driving torque and vehicle longitudinal acceleration. On the contrary, the longitudinal deformation of the tire tends to be smaller with the smaller adhesion coefficient, resulting in slighter fluctuation of drive torque and longitudinal acceleration. In addition, the black line under road D shows a slight fluctuation with different shape from others. It is because that tire excessive spin happens in the low adhesion condition. The road longitudinal force applied on the tire cannot balance the driving torque transferred from half-shaft, in which the slip ratio exceeds the critical value. Therefore, the longitudinal force decreases rapidly inducing a slight fluctuation of acceleration.

From the above analysis, we can see that the tire torsional stiffness and the road surface attachment greatly affect the longitudinal low-frequency vibration. Therefore, the two factors must be taken into account in the establishment of the control-oriented vehicle longitudinal vibration model.

3.3. Sensitivity Analysis of the Vehicle Body and the Suspension. As discussed before, the vertical vibration of the suspension and the tire, together with the longitudinal vibration between the frame and the wheel, have some contributions to vehicle longitudinal low-frequency vibration. However, the longitudinal vibration of the wheel, caused by the bushing, has very little effect on the longitudinal low-frequency vibration of the vehicle. This is because that the longitudinal stiffness of the tire and the bushing are both huge. The tire longitudinal stiffness is larger than 10^5 N/m and the bushing stiffness is larger than 10^7 N/m, which will induce high-frequency vibration of the wheel and vehicle body. Due to the relatively larger weight of the sprung mass, more than hundreds times than that of wheels, the high-frequency longitudinal vibration of the wheel has very little effect on the longitudinal low-frequency vibration of the sprung mass. In that condition, the longitudinal vibration of the wheel is synchronized with the sprung mass in low-frequency domain. In other words, the wheel hub and the sprung mass are connected rigidly in longitudinal direction. The influence

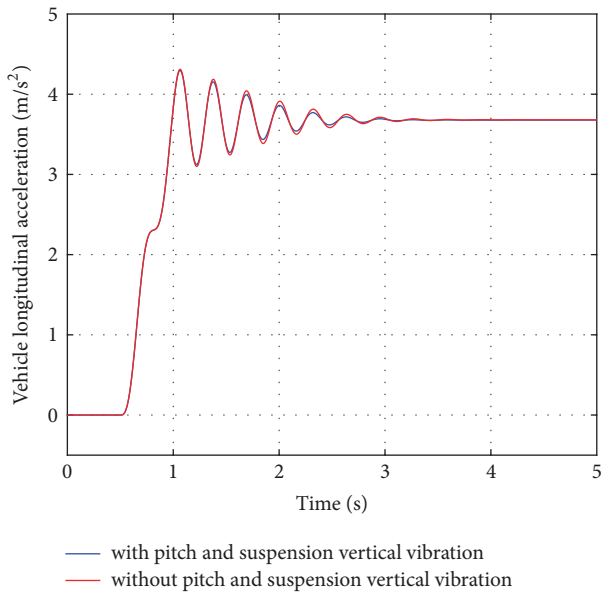

Figure 14: Longitudinal acceleration with/without pitch and suspension vertical vibration.

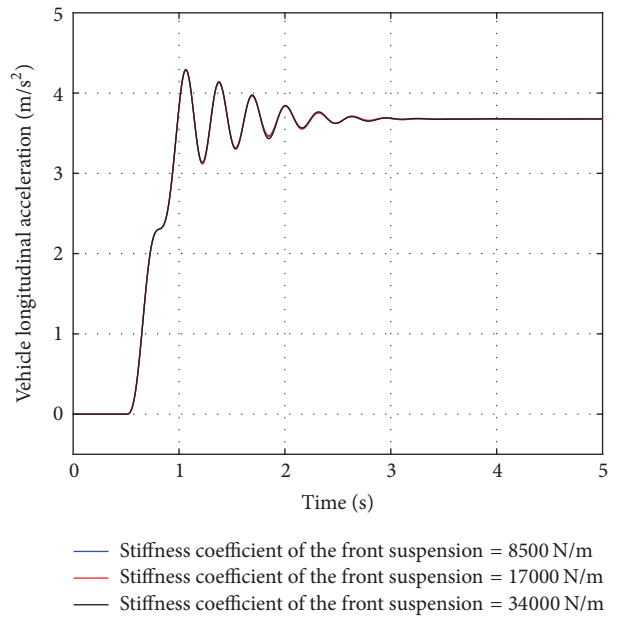

Figure 15: Sensitivity analysis: effect of the variation of suspension stiffness.

of the bushings is ignored. The former equation (14) is written as

$$\left(M_w + \frac{M_b}{2}\right)\ddot{x} = F_x, \tag{20}$$

where x is the longitudinal displacement of the vehicle.

Excluding the bushing, only the sensitivity of the vertical vibration of the suspension and the tire need to be analyzed. The vertical force applied on the tire from the ground fluctuates due to suspension vertical vibration, which makes the tire adhesion condition change. Thus the longitudinal force changes. Firstly, a model considering the suspension vertical vibration and the body pitch motion is simulated. For comparison, another vehicle model does not consider these, in which condition the vertical forces of front and rear wheels keep constant the same as those in stop condition. The longitudinal acceleration of the two models is shown in Figure 14.

In Figure 14, the red dotted line is the longitudinal acceleration without considering the pitch vibration, while the blue solid line considers the pitch vibration. It can be seen that the vertical vibration of the suspension has little effect on the frequency of the vehicle longitudinal vibration. In addition, the influence on the amplitude is very small.

In the range of normal value, 0.5, 1, and 2 times the nominal coefficients are set as system parameters in each simulation. Each stiffness coefficient of the front suspension is 5000 Nm/rad, 10000 Nm/rad, and 20000 Nm/rad, respectively. Sensitivity analysis results are shown in Figure 15.

Figure 15 shows that the three models with totally different values of suspension stiffness have almost the same longitudinal acceleration output. The longitudinal acceleration vibration is not sensitive to the variation of the suspension stiffness. In order to analyze the mechanism of this conclusion, some states of the vehicle are shown in Figure 16.

It can be seen from Figure 16(c) that the wheel vertical force fluctuates greatly in the vehicle model considering pitch vibration. Meanwhile, the steady-state value of the wheel vertical force is 800 N less than that of the vehicle model ignoring the pitch vibration. Due to the decrease of the vertical force, the tire is easier to slip under the same driving torque. Figure 16(a) shows that the tire slip ratio has a larger fluctuation amplitude and steady-state value under the influence of the suspension. However, the longitudinal force does not increase with the increase of the slip ratio and the longitudinal friction coefficient as shown in Figures 16(a), 16(b), and 16(d). The reason is that the road can provide the tire sufficient longitudinal force to balance the torque from half-shaft, but only when the slip ratio is lower than the critical value. Thus, a conclusion can be drawn that the suspension vertical and the vehicle body pitch vibrations have little effect on the longitudinal force when the slip ratio is lower than the critical value. In some exceptional conditions, such as low friction coefficient road, suspension vibration will have serious effect on the longitudinal force. This is because that tire slip ratio will exceed the critical value easily when the tire vertical force decreases. In that condition, the tire longitudinal force decreases into a steady value, which weakens acceleration fluctuation amplitude, as shown in Figure 17. A suspension with low stiffness could also cause the slip ratio to exceed the critical value, which will weaken acceleration fluctuation amplitude.

Although the tire vertical force fluctuates seriously in tip-in condition, caused by the vertical vibration of the suspensions and the tires, the tire longitudinal force is not influenced. The effect of the suspensions on the vehicle longitudinal vibration is negligible when the slip ratio is lower

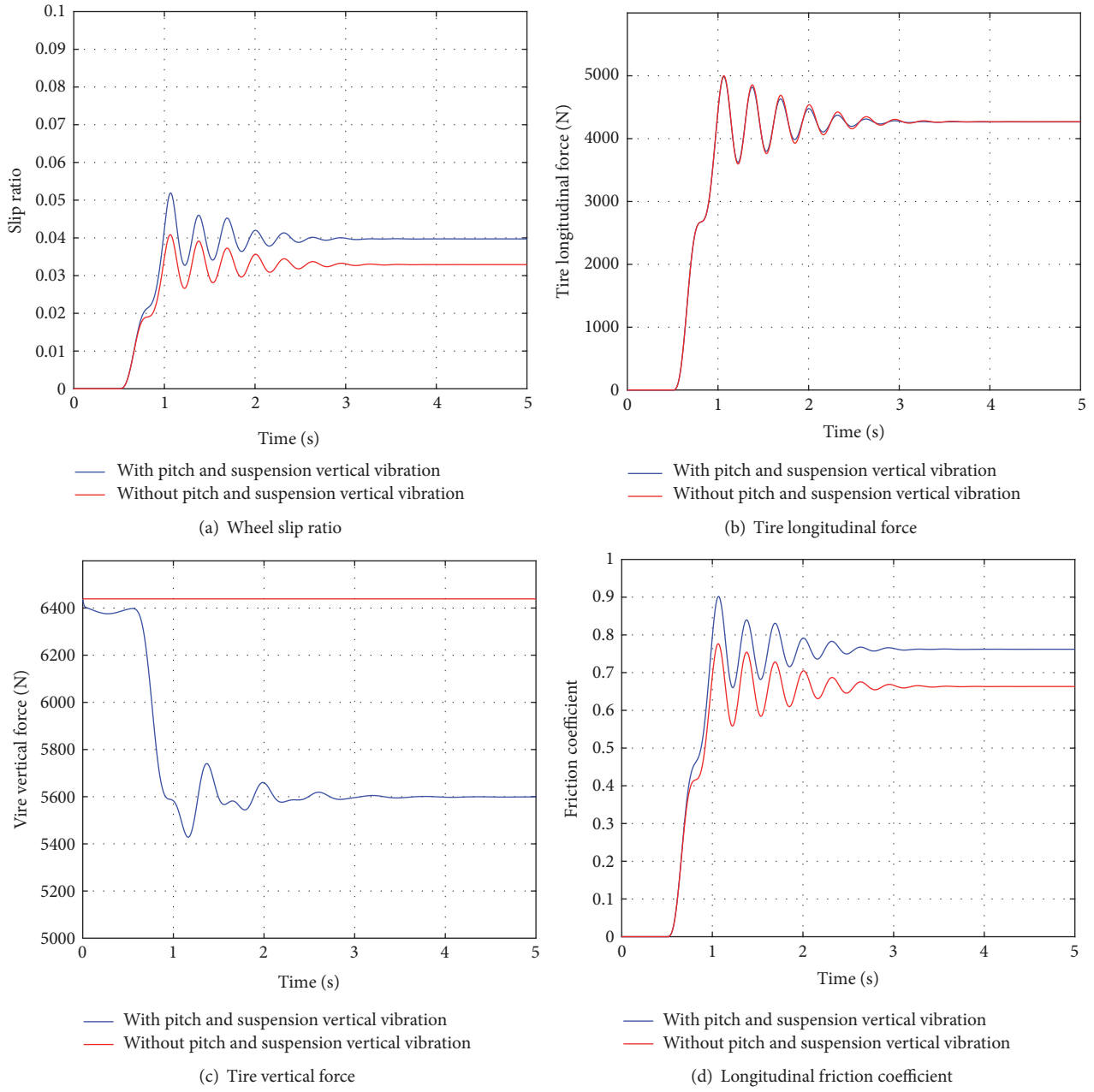

(a) Wheel slip ratio

(b) Tire longitudinal force

(c) Tire vertical force

(d) Longitudinal friction coefficient

Figure 16: States of vehicle model with/without considering suspension vertical vibration.

than the critical value. Therefore, the vertical vibration of the tires and the suspensions can be ignored in the establishment of the control-oriented vehicle longitudinal vibration model when the slip ratio is in the approximate linear region.

4. Reduced-Order Model for Longitudinal Vibration Control

To design a model-based active control algorithm, it is necessary to obtain a model which can reflect the dynamic process of the controlled object. The detailed model established above is not suitable for controller design due to the multiple degree-of-freedom and nonlinear tire force. This will make it difficult and complex to design control algorithms. In addition, it is not suitable for real-time computing due to its complexity. Therefore, a model, not only with a least degrees of freedom and linearization, but also ensuring a real reflection of dynamic process of vehicle longitudinal vibration, is needed. As the previous analysis, the clutch, the half-shaft, and the tire make great contributions to the longitudinal acceleration vibration. The stiffness and damping and the nonlinear part in these components should be taken into account to establish a reduced-order model reasonably. In this part, the model with multiple degrees of freedom and nonlinearity is reduced to two different linear models, respectively. One has two degrees of freedom and another has

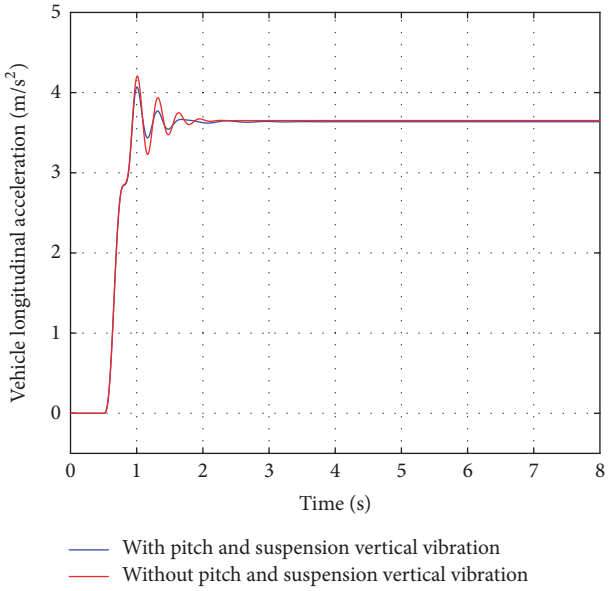

FIGURE 17: Longitudinal acceleration with/without pitch and suspension vertical vibration on low friction coefficient road.

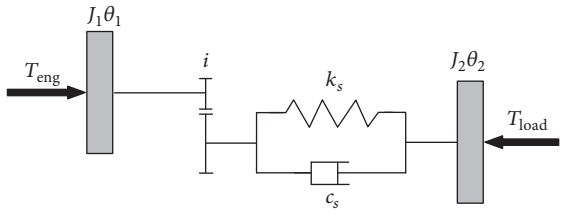

FIGURE 18: Structure of two degree-of-freedom vehicle longitudinal vibration model.

three degrees of freedom. The process and method of model order reduction and the parameters obtained method are also shown in this part.

4.1. Two-Degree-of-Freedom Model. A state space equation based on the two-degree-of-freedom model could has fewer state variables, which greatly simplifies the complexity of the controller. A two-degree-of-freedom vehicle longitudinal vibration model have been used in some literatures [14, 18, 20, 23, 24]. Lumped-mass method is used to reduce the order. Elastic components are concentrated as a torsion spring and damping system while rigid components with vital mass are concentrated to certain lumped mass. In this study, the torsional stiffness and damping of the clutch, half-shaft, and tire are simplified to a torsion spring and damping system while the mass of the engine flywheel, clutch, gearbox shaft, differential shaft, half-shaft, and hub are concentrated to a rotational inertia. Since the vibration of the suspensions has little effect on the vehicle longitudinal vibration from the previous analysis, the tire and the vehicle body are concentrated as a rotational inertia. The structure of the two-degree-of-freedom model is shown in Figure 18.

J_1 is the lumped rotational inertia of the engine flywheel, the clutch, the gearbox shaft, the differential shaft, the half-shaft, and the wheel hub. J_2 is the rotational inertia of the vehicle. k_s and c_s are the equivalent torsional stiffness and damping coefficient of the clutch, the half-shaft, and the tire. Parameters obtained method is shown in Section 4.3.1 below.

In tip-in condition, rolling resistance and air drag are small due to low speed. Vehicle load can be neglected and thus T_{load} is equal to zero. The equations for the two-degree-of-freedom model are

$$\begin{aligned} J_1\ddot{\theta}_1 &= T_e + T_s \cdot i, \\ J_2\ddot{\theta}_2 &= T_s - T_{\text{load}}, \\ T_s &= k_s\left(\frac{-\theta_1}{i} + \theta_2\right) + c_s\left(\frac{-\dot{\theta}_1}{i} + \dot{\theta}_2\right), \\ a_v &= r \cdot \ddot{\theta}_2. \end{aligned} \tag{21}$$

4.2. Three-Degree-of-Freedom Model. One function of the model is to predict the future outputs. In this study, the longitudinal vibration state is predicted based on the model using measured wheel speed as input. However, the wheel speed sensor measures the rotational speed of the hub rather than the tire. The hub speed has a large difference with the tire speed, especially in the tip-in condition. In addition, the tire rotation speed is not synchronous with that of the sprung mass due to the tire slip. Therefore, vehicle longitudinal vibration states cannot be obtained accurately from the model, which neglects the torsional stiffness and the tire slip, such as the two-degree-of-freedom model. The hub, the tire, and the sprung mass must be modeled separately in the new model. To establish this model, the dynamic relationship among the wheel hub, the tire, and the vehicle should be expressed in linear form.

The longitudinal force of tire can be calculated by

$$F_x = s_f \frac{\dot{\theta}_w - \dot{\theta}_v}{\dot{\theta}_v}. \tag{22}$$

s_f is the slope in the quasilinear area of the slip ratio-friction coefficient curve, as shown in Figure 19.

It can be seen that the longitudinal force is not linear with the vehicle speed $\dot{\theta}_v$ from equation (22) and Figure 19. However, the longitudinal low-frequency vibration mainly happens in 1st gear tip-in condition. The engine speed range is from 800 RPM to 3000 RPM, corresponding to 6.5 rad/s–24 rad/s in wheel speed. Since the speed variation is small, it is desirable to take a fixed vehicle speed for linearization. Therefore, (22) can be written as

$$F_x = c_v\left(\dot{\theta}_w - \dot{\theta}_v\right), \tag{23}$$

where $c_v = s_f/\dot{\theta}_{v0}$ and $\dot{\theta}_{v0}$ is a fixed value. Equation (23) shows that the tire longitudinal force is proportional to the difference between the wheel speed and the vehicle speed. This means a damping without mass can be equivalent to the connection between the wheel and the sprung mass. The damping coefficient is c_v.

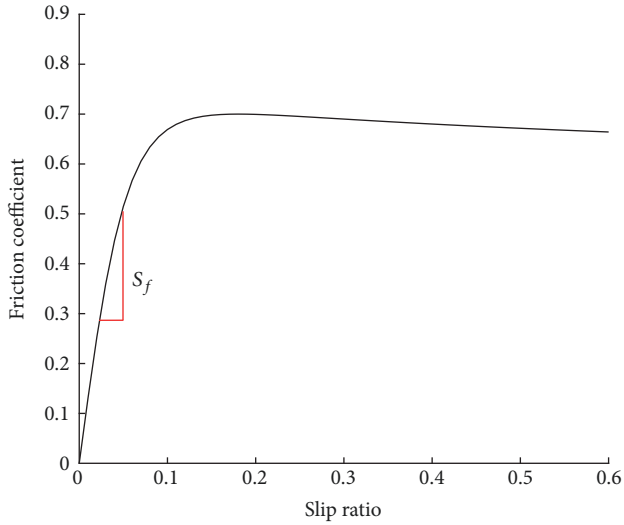

Figure 19: Slip ratio-friction coefficient curve.

Since the tire mass is much less than the sprung mass, the tire torsional stiffness k_v and the equivalent damping c_v can be combined in parallel form. The structure of the three-degree-of-freedom model is shown in Figure 20.

J_1 is the lumped rotational inertia of the engine flywheel, the clutch, the gearbox shaft, the differential shaft, and the half-shaft. J_2 is the hub (including the hub, the rim, and the brake disk) rotational inertia. J_3 is the lumped rotational inertia of the tire and the sprung mass. k_s and c_s are the equivalent torsional stiffness and damping coefficients of the clutch and the half-shaft.

The equations for the three-degree-of-freedom model are

$$\begin{aligned} J_1\ddot{\theta}_1 &= T_e + \frac{2T_s}{i}, \\ J_2\ddot{\theta}_2 &= T_s - T_v, \\ J_3\ddot{\theta}_3 &= T_v, \\ T_s &= k_s\left(\frac{-\theta_1}{i} + \theta_2\right) + c_s\left(\frac{-\dot{\theta}_1}{i} + \dot{\theta}_2\right), \\ T_v &= k_v\left(-\theta_2 + \theta_3\right) + c_v\left(-\dot{\theta}_2 + \dot{\theta}_3\right), \\ a_v &= r \cdot \ddot{\theta}_3. \end{aligned} \tag{24}$$

Parameters obtained method is shown in Section 4.3.2 below.

4.3. Model Parameters Estimation. Since structures and parameter meanings between the two reduced-order model are different, the estimation method of model parameters is different.

4.3.1. Parameter Estimation of Two-Degree-of-Freedom Model. The equivalent moment of inertia is obtained by the lumped-mass method. However, the moments of inertia of the clutch, the gearbox shaft, and the half-shaft are more than three orders of magnitude lower than that of the engine flywheel. In addition, these moments of inertia should be divided by the square of the gear ratio to lump to the engine side. Therefore, all these moments of inertia can be ignored except that of the engine flywheel. The tire and the sprung mass are lumped to one moment of inertia. The equations are

$$\begin{aligned} J_1 &= J_e, \\ J_2 &= J_{\text{tyre}} + \left(0.5m + m_{\text{tyre}}\right) \cdot r^2. \end{aligned} \tag{25}$$

The values of the equivalent torsional stiffness k_s and damping c_s are calculated by

$$\begin{aligned} \frac{T \cdot i}{k_s} &= \frac{T}{k_c \cdot i} + \frac{T \cdot i}{k_{\text{hs}}} + \frac{T \cdot i}{k_t}, \\ \frac{T \cdot i}{c_s} &= \frac{T}{c_c \cdot i} + \frac{T \cdot i}{c_{\text{hs}}} + \frac{T \cdot i}{c_t}, \end{aligned} \tag{26}$$

where $i = i_g \cdot i_d$. i_g is transmission ratio of the gearbox and i_d is transmission ratio of the differential.

4.3.2. Parameter Estimation of Three-Degree-of-Freedom Model. The values of the equivalent torsional stiffness k_s and damping c_s are calculated by

$$\begin{aligned} \frac{T \cdot i}{k_s} &= \frac{T}{k_c \cdot i} + \frac{T \cdot i}{k_{\text{hs}}}, \\ \frac{T \cdot i}{c_s} &= \frac{T}{c_c \cdot i} + \frac{T \cdot i}{c_{\text{hs}}}. \end{aligned} \tag{27}$$

The values of the equivalent moments of inertia are obtained by

$$\begin{aligned} J_1 &= J_e, \\ J_2 &= J_{\text{rim}}, \\ J_3 &= \left(0.5m + m_{\text{tyre}}\right) \cdot r^2, \end{aligned} \tag{28}$$

where J_e is the moment of inertia of engine flywheel. J_{rim} is the sum of the moments of inertia of the wheel hub, the rim, and the brake disk. m is the sprung mass. m_{tyre} is the tire mass. r is the wheel effective rolling radius.

In this model, the equivalent tire damping is proposed under the assumption of a fixed vehicle speed in tip-in condition. However, in different vehicle speed, the prediction accuracy of the model using this damping value needs to be verified. In addition, the slop s_f varies in different roads and, unfortunately, it cannot be obtained from the tire manufacturers easily. The above two factors affect the determination of the value of the tire equivalent damping. Here, parameter estimation method is used.

Firstly, it needs to determine the parameters to be estimated, the initial values, the inputs of the model, and the reference variables. In this case, the value of the equivalent tire damping c_v needs to be estimated and initial value is set to 5 Nm/(rad/s). The inputs are the engine torque with different slopes. The reference variables depend on the structure of

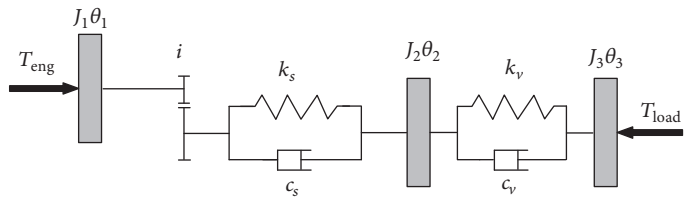

Figure 20: Structure of three-degree-of-freedom vehicle longitudinal vibration model.

the state space equation. This is because that the state space equation is needed to describe the dynamic process of the system based on the modern control theory. In this study, the engine speed, the wheel rim speed, and the vehicle speed are taken as the reference variables since they can reflect the dynamic process of real physical system and the longitudinal vibration. The estimated parameters, the inputs, and the reference variables are in the following state space equation (29), transformed from the model differential equation (24):

$$\begin{aligned} \dot{x} &= Ax + Bu, \\ y &= Cx, \end{aligned} \tag{29}$$

where

$$A = \begin{bmatrix} \frac{-2c_s}{i^2 J_1} & \frac{2c_s}{iJ_1} & 0 & \frac{-2k_s}{iJ_1} & 0 \\ \frac{c_s}{iJ_2} & \frac{-c_s - c_v}{J_2} & \frac{c_v}{J_2} & \frac{k_s}{J_2} & \frac{-k_v}{J_2} \\ 0 & \frac{c_v}{J_3} & \frac{-c_v}{J_3} & 0 & \frac{k_v}{J_3} \\ \frac{1}{i} & -1 & 0 & 0 & 0 \\ 0 & 1 & -1 & 0 & 0 \end{bmatrix}, \tag{30}$$

$$\begin{aligned} B &= \begin{bmatrix} \frac{1}{J_1} & 0 & 0 & 0 & 0 \end{bmatrix}', \\ C &= \begin{bmatrix} \frac{1}{i} & -1 & 0 & 0 & 0 \end{bmatrix}, \\ x &= \begin{bmatrix} x_1 & x_2 & x_3 & x_4 & x_5 \end{bmatrix}', \\ x_1 &= \dot{\theta}_1, \\ x_2 &= \dot{\theta}_2, \\ x_3 &= \dot{\theta}_3, \\ x_4 &= \frac{\theta_1}{i} - \theta_2, \\ x_5 &= \theta_2 - \theta_3. \end{aligned} \tag{31}$$

In (31), $\dot{\theta}_1$ is the engine speed. $\dot{\theta}_2$ is the driving wheel rim speed. $\dot{\theta}_3$ is the equivalent vehicle speed in wheel side. i is the transmission ratio from the engine to the wheel.

Secondly, a cost function is established as shown by

$$\begin{aligned} J = \sum_{\forall i} \Big\{ &\left(\dot{\theta}_{1\_d} - \dot{\theta}_{1\_r}\right)^2 + \left(\dot{\theta}_{2\_d} - \dot{\theta}_{2\_r}\right)^2 \\ &+ \left(\mathrm{acc}_d - \mathrm{acc}_r\right)^2 \Big\}, \end{aligned} \tag{32}$$

where $\forall i$ means the data in every acquisition step and $\mathrm{acc} = \ddot{\theta}_3 \cdot r$.

In (32), $\dot{\theta}_{1\_d}$, $\dot{\theta}_{2\_d}$ and acc_d are engine speed, wheel speed, and longitudinal acceleration, calculated by using (24). They are the outputs of the 3-dof model established by Matlab/Simulink in Section 5, shown as Figure 23. $\dot{\theta}_{1\_r}$, $\dot{\theta}_{2\_r}$, and acc_r are engine speed, wheel speed, and longitudinal acceleration, respectively, obtained from the detailed multi-degree-of-freedom vehicle longitudinal vibration model. The latter three variables are the reference signals. The aim is to make the cost function J close to its minimum value by adjusting the value of the equivalent tire damping. Here the nonlinear least square algorithm [25–27] is introduced to solve the problem. That algorithm is conducted to solve the optimal value in Matlab by using the nonlinear least square toolbox [28]. It uses $\dot{\theta}_{1\_d}$, $\dot{\theta}_{2\_d}$, acc_d, $\dot{\theta}_{1\_r}$, $\dot{\theta}_{2\_r}$, acc_r and initial value of the equivalent tire damping c_{v0} as inputs and calculates the optimal value of c_v as output, which makes the cost function J close to its minimum value.

Since different increase rates of engine torque have different impacts on the amplitude of longitudinal acceleration vibration, estimated results under a certain increase rate may not be able to meet the accuracy requirements in different torque increase rates. In addition, the reduced-order model cannot accurately reflect the vibration in the whole frequency range due to the few degrees of freedom. Therefore, it is necessary to design several experiments to estimate the parameters. The parameter values estimated in different groups are synthesized to obtain a final value. Considering the general tip-in process, the range of torque increase rate is 300–700 Nm/s. Therefore, three experiments are conducted with the torque increase rate of 300 Nm/s, 500 Nm/s, and 700 Nm/s, respectively. Arithmetic average of estimated parameter values from each experiment is considered as the final value. At last, torque increase rate of 400 Nm/s is used to verify the estimated parameter values.

The optimization trajectory of estimated parameter value is shown in Figure 21, which presents how the estimated parameter values change during the estimation.

As Figure 21 shows, the optimized values are 39.8 Nm/(rad/s), 44.2 Nm/(rad/s), and 51 Nm/(rad/s), respectively, in the three groups. The average value is 45 Nm/(rad/s).

Table 2: Trajectory of the cost function J.

Iteration	Group		
	Torque slope = 300	Torque slope = 500	Torque slope = 700
(1)	5.2255	15.7730	6.5047
(2)	4.0565	6.3970	4.2213
(3)	3.7978	4.1164	3.7021
(4)	3.7668	3.7841	3.6479
(5)	3.7661	3.7743	3.6477
(6)		3.7742	3.6476

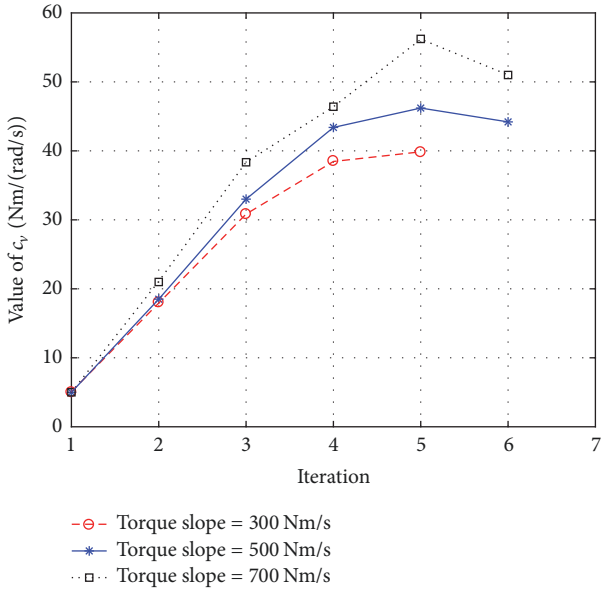

Figure 21: Parameter trajectories during the estimation.

Table 3: Parameters values of the two reduced-order models.

Parameter	Two-degree-of-freedom model	Three-degree-of-freedom model
J_1	0.134 kg·m^2	0.134 kg·m^2
J_2	82.156 kg·m^2	0.874 kg·m^2
J_3	-	81.110 kg·m^2
k_s	4069 Nm/rad	9718 Nm/rad
c_s	6.65 Nm/(rad/s)	19.88 Nm/(rad/s)
k_v	-	7000 Nm/rad
c_v	-	45 Nm/(rad/s)

The trajectory of the cost function J in the three groups is also shown in Table 2.

The reference variables including the engine speed $\dot{\theta}_1$, the driving wheel rim speed $\dot{\theta}_2$, and the longitudinal acceleration acc are also compared between the 3-dof model and the detailed model, as shown in Figure 22.

All the estimated parameter values of the two models are shown in Table 3.

5. Model Verification

The responses of the two reduced-order models are presented in this subsection. Compared with the response of the detailed vehicle model, accuracy of each reduced-order model is obtained and analyzed. All the models are built in Matlab/Simulink, as shown in Figure 23.

All the three models have the same input torque with increase rate of 400 Nm/s as shown in Figure 6.

5.1. Verification in Time Domain. Since the longitudinal acceleration and the speed difference are the indicators of longitudinal low-frequency vibration, the two variables are used to validate the reduced-order models. The two variables in reduced-order models are compared with those in the detailed model. The speed difference is defined as the difference between the engine flywheel speed divided by whole transmission ratio and wheel speed, written as $\Delta\dot{\theta} = \dot{\theta}_e/(i_g \cdot i_d) - \dot{\theta}_{\text{rim}}$.

Figure 24(a) shows the speed difference while Figure 24(b) shows the longitudinal acceleration. Red lines represent the two-degree-of-freedom model while blue lines represent the detailed model.

It can be seen from Figure 24(b) that the two-degree-of-freedom model generally fits the detailed model until the acceleration value reaches its first peak. The reduced-order model has large deviation in frequency and amplitude. The speed differences of the two models has large deviation in the whole time domain as shown in Figure 24(a). Actually, the reduced-order model is a simple spring and damper system. From Figure 24 a conclusion can be drawn that the two-degree-of-freedom model ignoring the tire slip is an underdamped system. This is because energy dissipates when the tire slip happens, which is equivalent to damping. As in a previous analysis, the tire slip has great influence on longitudinal vibration. Therefore, acceleration of the model ignoring the tire slip keeps vibrating in a longer time, as shown in Figure 24. Consequently, the two-degree-of-freedom vibration model is not able to reflect the vehicle longitudinal low-frequency vibration.

Figure 25(a) shows the speed difference while Figure 25(b) shows the longitudinal acceleration. Red lines represent the three-degree-of-freedom model while blue lines represent the detailed model.

In the aspect of the frequency and amplitude of the vibration, the three-degree-of-freedom model can reflect

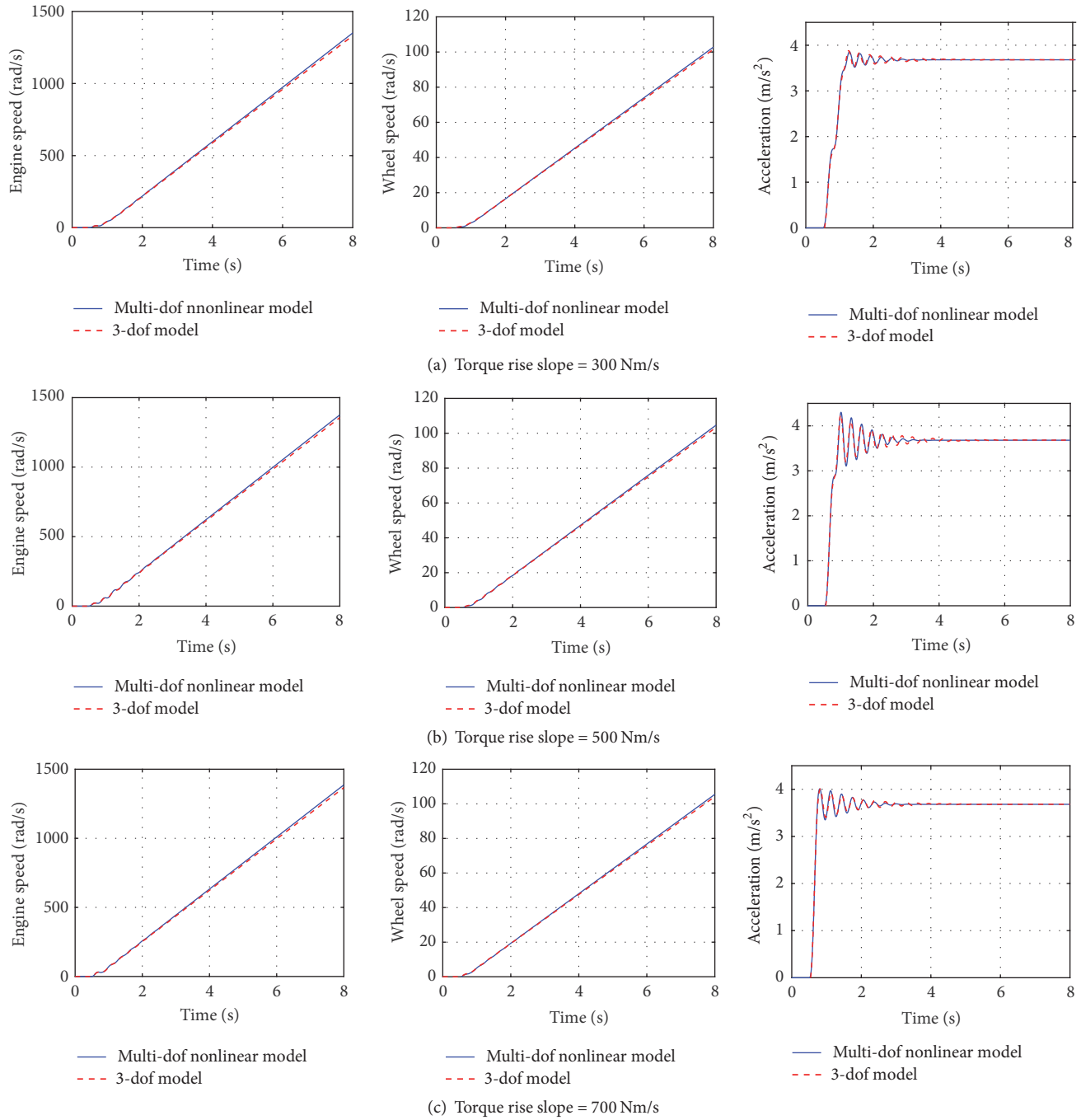

(a) Torque rise slope = 300 Nm/s

(b) Torque rise slope = 500 Nm/s

(c) Torque rise slope = 700 Nm/s

Figure 22: Reference variables compared between the 3-dof model and the detailed model.

the longitudinal vibration more accurately. Although the vibration of the three-degree-of-freedom model attenuates slower after the fifth peak, this model has enough accuracy if the control algorithm to be designed will suppress the vibration before the first five vibration peaks. In addition, feedback correction can be added to the control algorithm to correct the errors. Therefore, an accurate reduced-order model is obtained.

5.2. Error Analysis. The errors of the two reduced-order models are shown in Figure 26. Red lines represent the two-degree-of-freedom model while blue lines represent the three-degree-of-freedom model.

Figure 26 shows that errors of three-degree-of-freedom model are smaller than that of two-degree-of-freedom model, no matter speed difference or acceleration. Table 4 shows the error statistic. Maximum absolute error is defined as the maximum value of absolute errors in all simulation steps. Accumulative absolute error is defined as the arithmetic sum of errors in all simulation steps. The size of simulation step is 0.001 and the simulation time is 8 s.

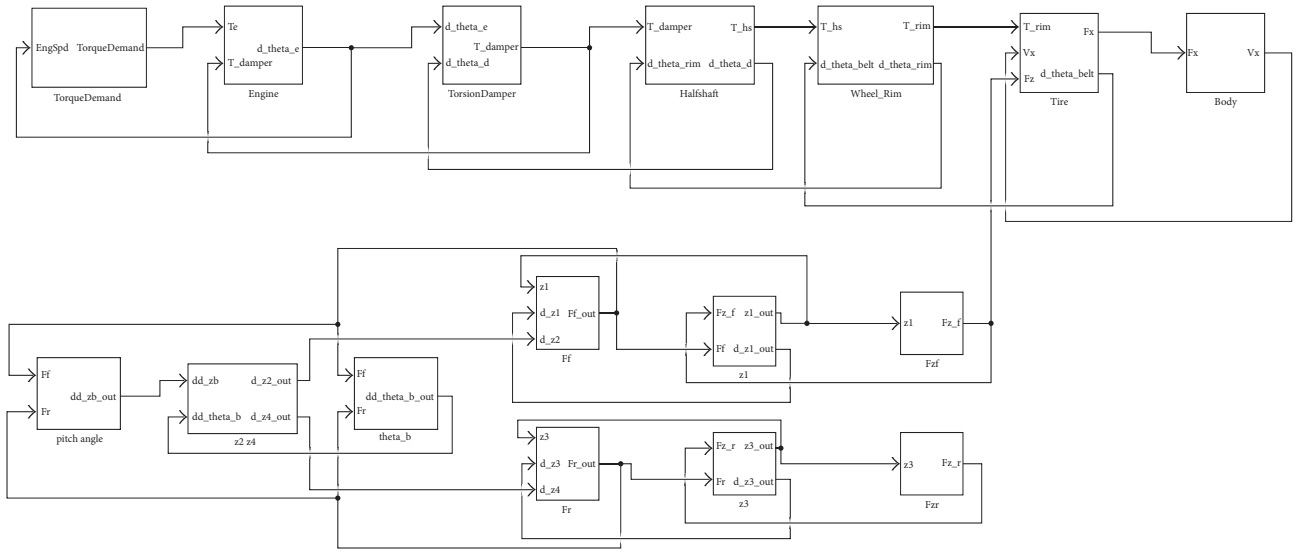

(a) Multi-degree-of-freedom nonlinear detailed longitudinal vibration model

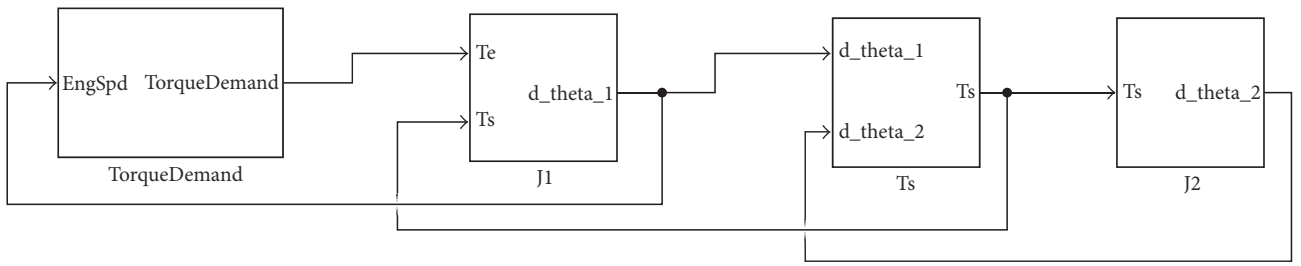

(b) Two-degree-of-freedom longitudinal vibration model

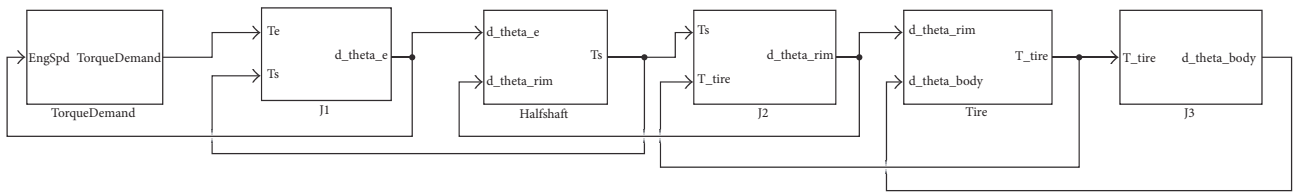

(c) Three-degree-of-freedom longitudinal vibration model

Figure 23: Vehicle longitudinal vibration model in Simulink.

It can be seen from Table 4 that three-degree-of-freedom model fits the detailed model more, no matter maximum absolute error or accumulative absolute error.

5.3. Verification in Frequency Domain. Considering the considerable influence of the torque increase time on longitudinal vibration, frequency analysis is needed to validate the accuracy in different torque increase rates. Unit pulse excitation is set as inputs into the three models. Frequency responses are obtained as shown in Figure 27.

It can be seen from Figure 27 that the detailed model and the three-degree-of-freedom model have good coincidence in the interested frequency range (0–10 Hz). Their peaks are at frequency point of 3.175 Hz, with few deviations. However, the frequency response of the two-degree-of-freedom model is different from that of the detailed model. Their peaks are in different frequency points.

6. Conclusion

(1) A detailed multi-degree-of-freedom nonlinear vehicle longitudinal vibration model is established, considering the torsional vibration of the transmission system and the tire, the tire nonlinear longitudinal force, and the pitch and vertical vibration of the vehicle. This model can reflect the characteristics of the vehicle longitudinal low-frequency vibration. Based on this model, the mechanism of the longitudinal low-frequency vibration is revealed. As a result, the torsional stiffness variation of the half-shaft and the tire and the tire slip characteristic has obvious effect on vehicle longitudinal low-frequency vibration while the torsional stiffness variation of clutch has negligible effect on that by sensitivity analysis. In addition, the suspension vertical vibration and the body pitch vibration have negligible influence on longitudinal low-frequency vibration when the driving wheel does not reach the critical value.

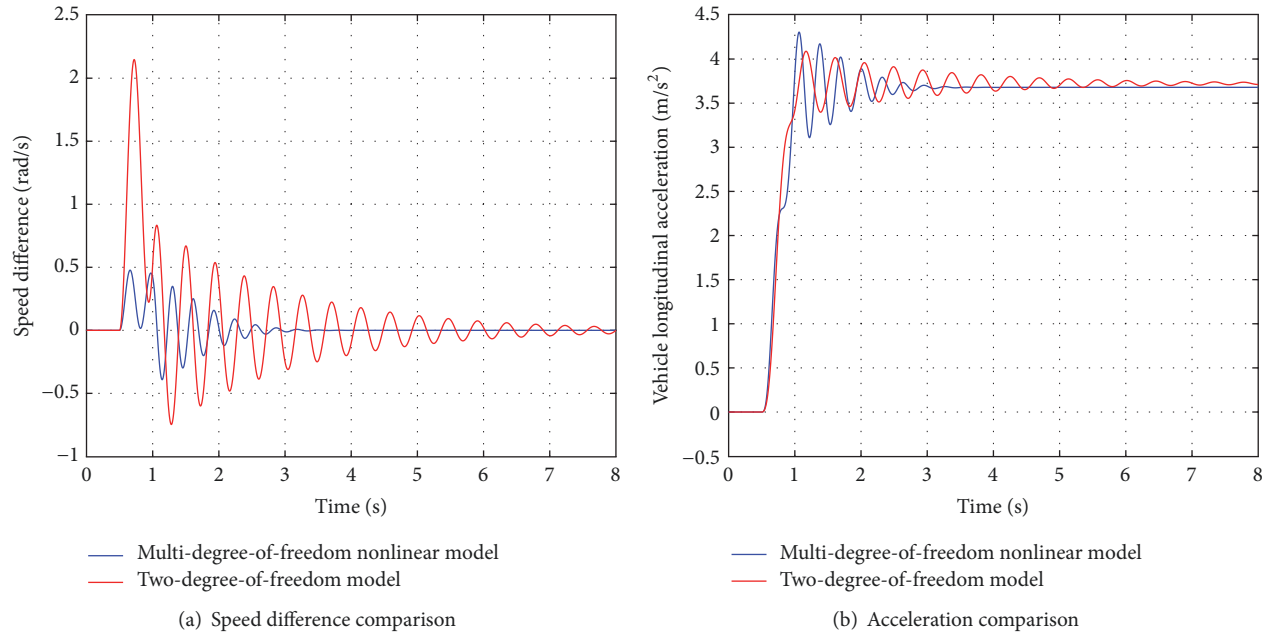

(a) Speed difference comparison (b) Acceleration comparison

Figure 24: Two-degree-of-freedom model verification.

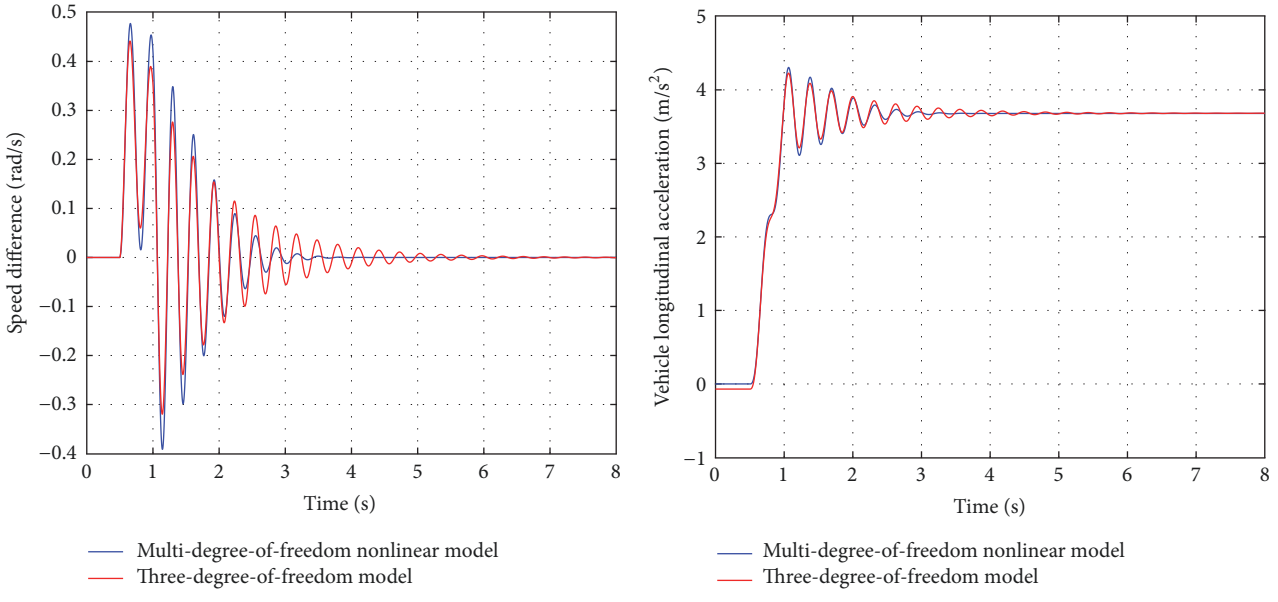

(a) Speed difference comparison (b) Acceleration comparison

Figure 25: Three-degree-of-freedom model verification.

Table 4: Error statistic.

Error type	Two-degree-of-freedom model	Three-degree-of-freedom model
Maximum absolute error of acceleration	0.9006	0.1102
Accumulative absolute error of acceleration	869.2987	164.0155
Maximum absolute error of speed difference	1.8781	0.0771
Accumulative absolute error of speed difference	1535.3	102.0286

Table 5: Symbol and parameter value.

Symbol	Description	Value	Unit
k_c	Torsional stiffness coefficient of the clutch	$2e3$	Nm/rad
c_c	Torsional damping coefficient of the clutch	20	Nm/(rad/s)
k_{hs}	Torsional stiffness coefficient of the half-shaft	$1e4$	Nm/rad
c_{hs}	Torsional damping coefficient of the half-shaft	40	Nm/(rad/s)
k_{sf}	Vertical stiffness coefficient of the front suspension	$9e4$	N/m
k_{sr}	Vertical stiffness coefficient of the rear suspension	$9e4$	N/m
c_{sf}	Vertical damping coefficient of the front suspension	$3e3$	N/(m/s)
c_{sr}	Vertical damping coefficient of the rear suspension	$3e3$	N/(m/s)
k_{tf}	Vertical stiffness coefficient of the front tire	$1.92e5$	N/m
k_{tr}	Vertical stiffness coefficient of the rear tire	$1.92e5$	N/m
k_t	Torsional stiffness coefficient of the tire	$7e3$	Nm/rad
c_t	Torsional damping coefficient of the tire	10	Nm/(rad/s)
k_{bl}	Stiffness coefficient of the bushing connecting the wheel and the sprung mass	$1e7$	N/m
c_{bl}	Damping coefficient of the bushing connecting the wheel and the sprung mass	$2e3$	N/(m/s)
J_e	Mass moment of inertia of the engine flywheel	0.1322	kg·m^2
J_c	Mass moment of inertia of clutch	$2e-3$	kg·m^2
J_{g1}	Mass moment of inertia of gearbox input shaft and gears on it	$3.46e-4$	kg·m^2
J_{g2}	Mass moment of inertia of gearbox output shaft and gears on it	$6.67e-4$	kg·m^2
J_{df}	Mass moment of inertia of the differential output shaft	0.0784	kg·m^2
J_{d}	Equivalent mass moment of inertia of the engine flywheel in half-shaft side	0.4934	kg·m^2
J_{rim}	Moment of inertia of the wheel hub, rim and brake disk	0.1713	kg·m^2
J_{tire}	Moment of inertia of the tire	1.0457	kg·m^2
M_w	Mass of the wheel	5	kg
M_b	Mass of the vehicle	2300	kg
i_g	Reduction ratio of the gearbox	3.2	1
i_{df}	Reduction ratio of the differential	4.1	1
a	Distance between the front wheel center and the vehicle mass center in x direction	1.2	m
b	Distance between the rear wheel center and the vehicle mass center in x direction	1.5	m
h	Height of the vehicle mass center	0.5	m
r	Wheel effective rolling radius	0.265	m
θ_e	Angular displacement of the engine flywheel	-	rad
θ_{g1}	Angular displacement of the gearbox input shaft	-	rad
θ_{df}	Angular displacement of the differential output shaft	-	rad
$\theta_{\mathrm{rim}r}$	Angular displacement of the right wheel hub	-	rad
$\theta_{\mathrm{rim}l}$	Angular displacement of the left wheel hub	-	rad
θ_{wr}	Angular displacement of the right tire	-	rad
θ_{wl}	Angular displacement of the left tire	-	rad
θ_v	Equivalent vehicle displacement in the wheel side	-	rad
θ_b	Pitch angular displacement of the vehicle	-	rad
z_b	Vertical displacement of the vehicle body	-	m
z_{tf}	Vertical displacement of the front tire	-	m
z_{sf}	Vertical displacement of the front suspension	-	m
z_{tr}	Vertical displacement of the rear tire	-	m
z_{sr}	Vertical displacement of the rear suspension	-	m
x_1	Longitudinal displacement of the wheel center	-	m
x_2	Longitudinal displacement of the vehicle mass center	-	m
T_e	Effective output torque of the engine flywheel	-	Nm
T_c	Effective output torque of the clutch	-	Nm
T_g	Effective output torque of the gearbox output shaft	-	Nm
T_{hs}	Torque of the half-shaft	-	Nm

Table 5: Continued.

Symbol	Description	Value	Unit
T_{hsr}	Torque of the right half-shaft	-	Nm
T_{hsl}	Torque of the left half-shaft	-	Nm
T_{tire}	Torque of the tire	-	Nm
T_r	Rolling resistance torque of the tire	-	Nm
T_{tf}	Front wheel driving torque from road	-	Nm
F_x	Longitudinal force of the tire	-	N
F_z	Vertical force of the tire	-	N
F_b	Longitudinal force of the bushing between the wheel and the sprung mass	-	N
F_f	Vertical force of the front suspension	-	N
F_r	Vertical force of the rear suspension	-	N
s_t	Tire slip ratio	-	1
s_f	Slope in the quasilinear area of the slip ratio-friction coefficient curve	-	1
B, C, D	Parameters of the Magic Tire Formula	-	1

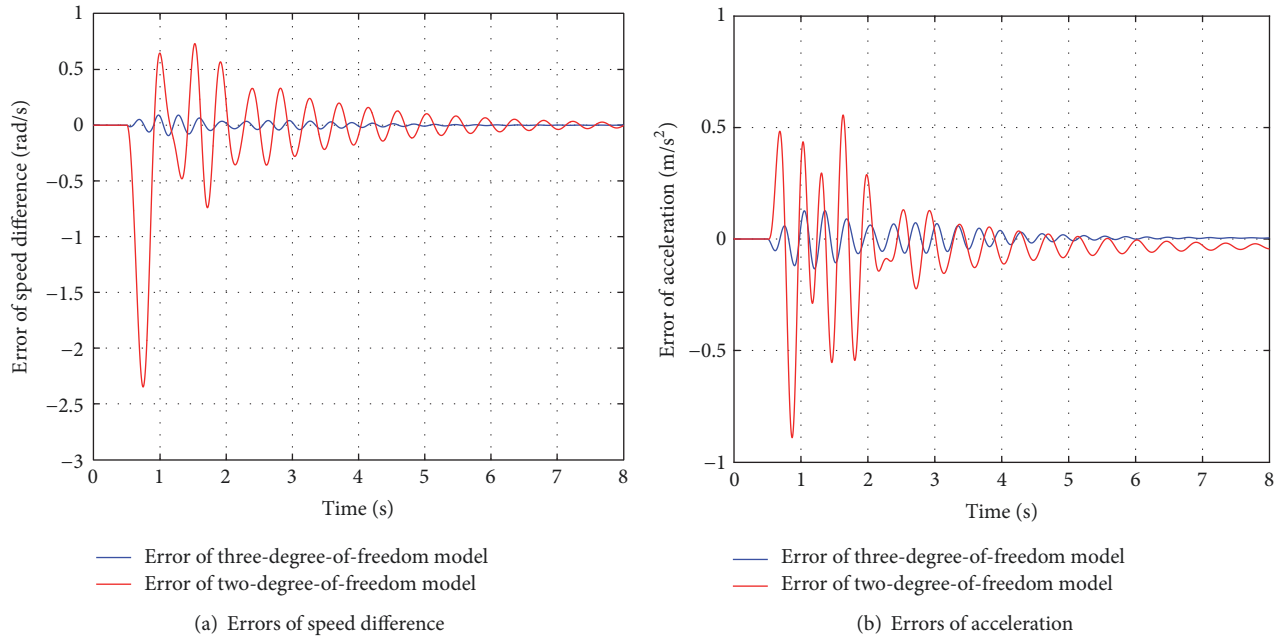

(a) Errors of speed difference

(b) Errors of acceleration

Figure 26: Errors of the two reduced-order models.

(2) A control-oriented linear model with three degrees of freedom is established. The order of the coupling system is reduced without losing important influence factors such as torsional vibration of the transmission and the tire. The nonlinear longitudinal force of the tire is linearized as an equivalent damper. The moments of inertia of the engine flywheel, the wheel hub (including rim, hub, and brake disk), and the equivalent moment of inertia of vehicle in wheel side compose the three degrees of freedom. The equivalent stiffness and damping coefficients between the flywheel and the wheel hub are derived from the stiffness and damping of the clutch and the half-shaft and those between the hub and vehicle are derived from the tire torsional stiffness and equivalent slip damping.

(3) Estimation method of model parameters is proposed for the reduced-order model. The torsional moments of inertia and the equivalent stiffness and damping coefficients are derived by lumped-mass method. The equivalent slip damping coefficient is estimated accurately by optimizing a designed penalty function.

(4) The three-degree-of-freedom model has a strong agreement with the detailed multi-degree-of-freedom nonlinear model. The time domain responses, error analysis, and frequency responses results show that the three-degree-of-freedom model fits the detailed model more than the two-degree-of-freedom model. The three-degree-of-freedom model can truly reflect the dynamics of vehicle longitudinal low-frequency vibration. It has the characteristics of linearity

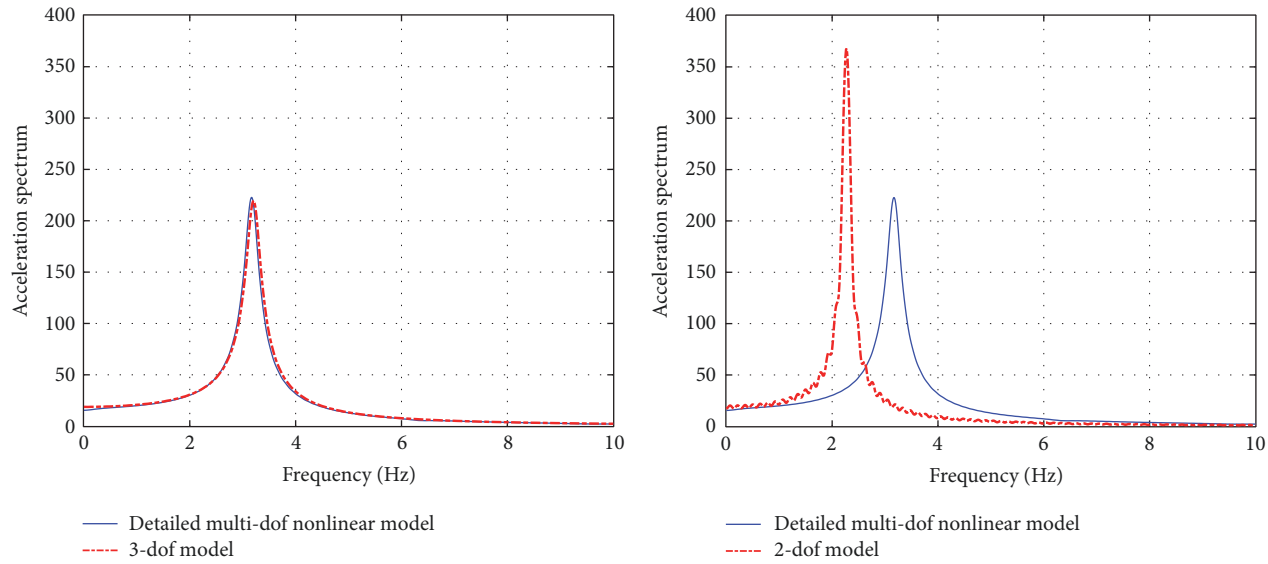

(a) Comparison between detailed model and three-degree-of-freedom model

(b) Comparison between detailed model and two-degree-of-freedom model

Figure 27: Frequency characteristics.

and few freedoms, which is suitable as a control-oriented model.

Conflicts of Interest

The authors declare that there are no conflicts of interest regarding the publication of this paper.

Acknowledgments

The authors would like to acknowledge the National Natural Science Foundation of China for financially supporting this research under Projects no. 51475043 and no. 50975026.

References

[1] Z. Wei, K. Hailin, and L. Chengde, "Analysis of vehicle surge," *Autornotive Engineering*, vol. 24, pp. 10–14, 2002.

[2] A. Albers, C. Zingel, J. Zehetner, and K. Meitz, "Influence of low-frequency powertrain-vibrations on driveability- assessments," *SAE Technical Papers*, 2010.

[3] J. M. Griffin, *Handbook of Human Vibration*, Academic press, 2012.

[4] E. M. A. Rabeih and D. A. Crolla, "Coupling of driveline and body vibrations in trucks," in *Proceedings of the 1996 SAE International Truck and Bus Meeting and Exposition*, vol. 1203, SAE Conf. Trans., Detroit, 1996.

[5] A. Sorniotti, "Driveline modeling, experimental validation and evaluation of the influence of the different parameters on the overall system dynamics," *SAE Technical Papers*, 2008.

[6] A. R. Crowther and N. Zhang, "Torsional finite elements and nonlinear numerical modelling in vehicle powertrain dynamics," *Journal of Sound and Vibration*, vol. 284, no. 3–5, pp. 825–849, 2005.

[7] Y.-C. Choi, H.-B. Song, J.-H. Lee, and H.-S. Cho, "An experimental study for drivability improvements in vehicle acceleration mode," *Proceedings of the Institution of Mechanical Engineers, Part D: Journal of Automobile Engineering*, vol. 217, no. 7, pp. 623–631, 2003.

[8] M. Bartram, G. Mavros, and S. Biggs, "A study on the effect of road friction on driveline vibrations," *Proceedings of the Institution of Mechanical Engineers, Part K: Journal of Multi-body Dynamics*, vol. 224, no. 4, pp. 321–340, 2010.

[9] J. S. Bang, Y.-K. Ko, and T.-H. Jung, "The Active Damping Control to Reduce Driveline Oscillations for Electric Vehicles Using Wheel Speeds," *SAE Technical Papers*, vol. 2015-, no. April, 2015.

[10] L. Jin and O. Minggao, "A Study on Surge Control Strategy for Diesel Powertrain," *Automotive Engineering*, vol. 28, pp. 238–241, 2006.

[11] R. Daumer, E. Feldmann, M. Person, E. Wild, and M. Zechnall, "System for damping bucking oscillations of an automobile engine," *Google Patents*, 1985.

[12] J. Fredriksson, H. Weiefors, and B. Egardt, "Powertrain control for active damping of driveline oscillations," *Vehicle System Dynamics*, vol. 37, no. 5, pp. 359–376, 2010.

[13] C. Y. Mo, A. J. Beaumount, and N. N. Powell, "Active control of driveability," *SAE Technical Papers*, 1996.

[14] J. Baumann, D. D. Torkzadeh, A. Ramstein, U. Kiencke, and T. Schlegl, "Model-based predictive anti-jerk control," *Control Engineering Practice*, vol. 14, no. 3, pp. 259–266, 2006.

[15] P. Templin and B. Egardt, "A powertrain LQR-torque compensator with backlash handling," *Oil & Gas Science and Technology - Revue d'IFP Energies nouvelles*, vol. 66, no. 4, pp. 645–654, 2011.

[16] M. Pettersson and L. Nielsen, "Diesel engine speed control with handling of driveline resonances," *Control Engineering Practice*, vol. 11, no. 3, pp. 319–328, 2003.

[17] M. Berriri, P. Chevrel, and D. Lefebvre, "Active damping of automotive powertrain oscillations by a partial torque compensator," *Control Engineering Practice*, vol. 16, no. 7, pp. 874–883, 2008.

[18] P. Templin and B. Egardt, "An LQR torque compensator for driveline oscillation damping," in *Proceedings of the 2009 IEEE International Conference on Control Applications, CCA '09*, pp. 352–356, Petersburg, Russia, 2009.

[19] S. Richard, P. Chevrel, and B. Maillard, "Active control of future vehicles drivelines," in *Proceedings of the The 38th IEEE Conference on Decision and Control (CDC)*, pp. 3752–3757, Phoenix, AZ, USA, December 1999.

[20] M. Grotjahn, L. Quernheim, and S. Zemke, "Modelling and identification of car driveline dynamics for anti-jerk controller design," in *Proceedings of the 2006 IEEE International Conference on Mechatronics, ICM*, pp. 131–136, Budapest, Hungary, 2006.

[21] R. S. Sharp and C. J. Jones, "Self-excited Vibrations of Truck Tandem Axle Suspension and Transmission Systems," *Vehicle System Dynamics*, vol. 10, no. 2-3, pp. 201-202, 1981.

[22] H. B. Pacejka, "Tyre factors and front wheel vibrations," *International Journal of Vehicle Design*, vol. 1, no. 2, pp. 97–119, 1980.

[23] X. Lu, H. Chen, H. Zhang, P. Wang, and B. Gao, "Design of model predictive controller for anti-jerk during tip-in/out process of vehicles," in *Proceedings of the 30th Chinese Control Conference, CCC 2011*, pp. 3395–3400, chn, July 2011.

[24] K. Moriya, Y. Ito, Y. Inaguma, and E. Sato, "Design of the surge control method for the electric vehicle powertrain," *SAE Technical Papers*, 2002.

[25] K. Levenberg, "A method for the solution of certain non-linear problems in least squares," *Quarterly of Applied Mathematics*, vol. 2, pp. 164–168, 1944.

[26] D. Marquardt, "An algorithm for least-squares estimation of nonlinear parameters," *SIAM Journal on Applied Mathematics*, vol. 11, no. 2, pp. 431–441, 1963.

[27] J. J. Moré, "The Levenberg-Marquardt Algorithm: Implementation and Theory," in *Numerical Analysis*, G. A. Watson, Ed., Lecture Notes in Mathematics 630, pp. 105–116, Springer Verlag, 1977.

[28] Matlab Optimization Toolbox, https://www.mathworks.com/help/optim/ug/lsqnonlin.html.